ADVANCED MATERIALS
www.advmat.de

# Advancing Next-Gen Energy Storage with Single-Atom Materials

*Jianan Gu, Yuanfu Ren, Zhi-Peng Wu, Meicheng Li,* Zhiping Lai, Husam N. Alshareef, and Huabin Zhang**

**Single-atom materials (SAMs) are a fascinating class of nanomaterials with exceptional catalytic properties, offering immense potential for energy storage and conversion. This work explores their advantages, challenges, and underlying mechanisms, providing valuable insights for rational design. By precisely controlling active sites, SAMs enable efficient charge and energy transfer, ultimately enhancing system performance. In applications such as metal-ion batteries, supercapacitors, metal anodes, Li–S batteries, Na–S batteries, and metal–air batteries, SAMs effectively address key challenges, including volume change, dendrite formation, and capacity fading. Their unique electronic and structural properties also make them highly efficient electrocatalysts, demonstrating remarkable activity and selectivity in lithium polysulfide, oxygen reduction, and carbon dioxide reduction reactions. Finally, the challenges and future prospects of SAMs in the energy storage field are discussed. With ongoing research and development, SAMs are poised to revolutionize the field, serving as foundational elements in the transition to sustainable and clean energy.**

## 1. Introduction

Climate change is a global crisis demanding immediate attention. Rising greenhouse gas emissions involving $CO_2$ imperil ecosystems worldwide.[1,2] To mitigate these threats, advancing renewable energy technologies is imperative. Key innovations in the field of energy storage include metal-ion batteries,[3–6] Li–S batteries,[7–9] Li–$O_2$ batteries,[10–12] and Li–$CO_2$ batteries,[13–16] promising a cleaner energy future. However, challenges in these battery systems are still existing, including sluggish metal ion diffusion and low reaction kinetics.[17,18] Specially, metal-ion batteries (e.g., Li/Na/K/Zn-ion) face challenges such as sluggish ion diffusion kinetics, structural instability during cycling, and limited theoretical capacity. Li–S batteries suffer from the notorious polysulfide shuttle effect and poor sulfur conductivity.[19] Li–$O_2$ batteries are hindered by the insulating nature of discharge products ($Li_2O_2$) and sluggish oxygen reduction/evolution reactions (ORR/OER). Li–$CO_2$ batteries struggle with the irreversible decomposition of $Li_2CO_3$ and low catalytic efficiency for $CO_2$ reduction. These shared issues, such as, slow reaction kinetics, unstable interfaces, and material degradation, highlight the urgent need for advanced materials to address these bottlenecks. Researchers are exploring novel materials and designs to enhance battery performance. Recently, there has been a surge in exploring diverse materials with distinctive crystal structures, morphologies, and chemical compositions for electrode applications across a wide range of energy storage devices.[20–22]

Among the numerous materials explored, single-atom materials (SAMs) stand out as an intriguing class, possessing good properties and unique catalytic capabilities. They hold great promise for diverse energy storage systems.[23–27] SAMs exhibit high utilization of active materials and remarkable electrochemical activity, hastening reactions and lowering activation energy. Moreover, their isolated active sites minimize undesirable side reactions, enhancing process selectivity. With precise control over active sites, SAMs enable tailored charge and energy transfer, boosting overall system efficiency.[28–31] However, a deeper understanding of the mechanisms of SAMs in various energy storage systems, along with addressing the associated challenges, requires further comprehensive investigation.

Herein, we provide an overview and delve into the latest advancements in the diverse SAMs and their application in energy storage (**Figure 1**). We commence by examining the advantages, challenges, and operation mechanisms of SAMs in energy systems. Subsequently, we investigate their specific roles in

J. Gu, Y. Ren, Z.-P. Wu, Z. Lai, H. N. Alshareef, H. Zhang
Center for Renewable Energy and Storage Technologies (CREST)
Physical Science and Engineering Division
King Abdullah University of Science and Technology (KAUST)
Thuwal 23955–6900, Saudi Arabia
E-mail: huabin.zhang@kaust.edu.sa

J. Gu, Y. Ren, Z.-P. Wu, H. Zhang
KAUST Catalysis Center
Physical Sciences and Engineering Division
King Abdullah University of Science and Technology
Thuwal 23955, Saudi Arabia

J. Gu, M. Li
State Key Laboratory of Alternate Electrical Power System with Renewable Energy Sources
School of New Energy
North China Electric Power University
Beijing 100096, China
E-mail: mcli@ncepu.edu.cn

The ORCID identification number(s) for the author(s) of this article can be found under https://doi.org/10.1002/adma.202505009

**DOI: 10.1002/adma.202505009**

 

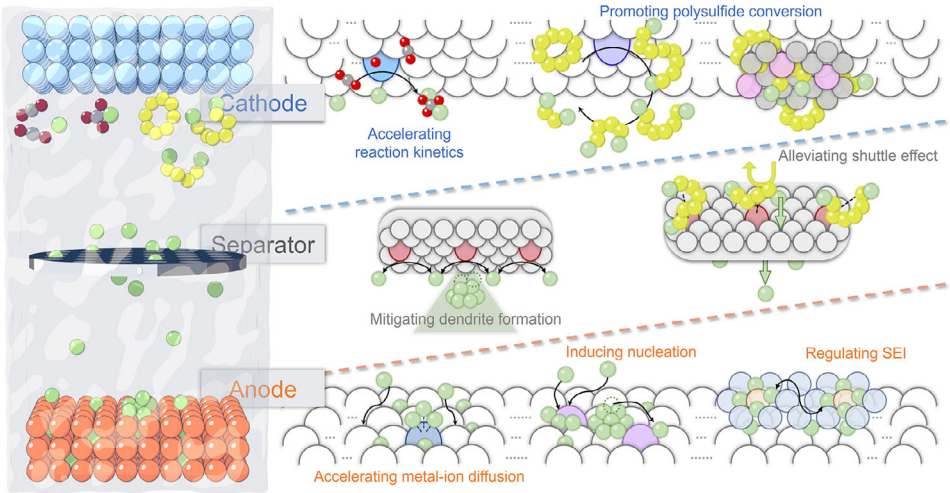


**Figure 1.** Schematic illustration of single-atom materials used in the field of energy storage as well as its relevant operation mechanism.

electronic energy storage. Endowed with unique electronic and structural attributes, these materials exhibit exceptional catalytic activity and selectivity, paving the way for more efficient energy processes. With ongoing research and development, SAMs are primed to transform the electronic energy storage landscape.

## 2. Advantages and Challenges of SAMs in Energy Storage Systems

In the realm of energy storage technologies, lithium-ion batteries (LIBs) reign supreme, renowned for their widespread utility with high-energy-density and relatively safe operation.[32–35] Yet, meeting escalating demands for enhanced energy and power densities remains a challenge. Furthermore, the scarcity of lithium resources and escalating prices have spurred exploration into alternative battery technologies.[36–39] This exploration encompasses sodium-ion batteries (SIBs),[36–39] potassium-ion batteries (PIBs),[40–43] aqueous zinc-ion batteries (ZIBs),[44–47] Li–S batteries,[48–51] metal–air batteries,[52–55] and Li–$CO_2$ batteries.[56–60] Each technology confronts its unique set of hurdles. For instance, SIBs and PIBs contend with voluminous electrode expansion due to larger metal ion radii ($Na^+$ and $K^+$) compared to $Li^+$.[61–64] For Li–S batteries, unregulated expansion of Li dendrites on the anode poses a formidable challenge, risking breaches in the battery separator and triggering internal short circuits.[65–67] Additionally, the S cathode encounters hurdles involving the dissolution and shuttle effect of lithium polysulfides (LiPSs), along with sluggish kinetic in their conversion to $Li_2S$.[68–71] Metal–air batteries, on the other hand, face obstacles in achieving efficient oxygen reduction reaction (ORR)[72–75] and carbon dioxide reduction reaction ($CO_2$RR)[76–79] catalysis. These challenges, encompassing sluggish ion diffusion, notorious dendrite formation, low reaction kinetics, and slow catalytic conversion, underscore the imperative of addressing them to propel energy storage technologies forward.

### 2.1. Advantages of SAMs

After over a decade of development, SAMs have emerged as versatile tools across diverse fields, prominently in the energy storage field (**Figure 2**). Their exceptional electrochemical activity, stemming from isolated active sites at the atomic scale,[80] distinguishes SAMs from conventional materials. Unlike bulk structures, SAMs optimize each active site, ensuring maximal utilization and efficient reactant interaction during electrochemical processes. Their high electrochemical activity owes to unique electronic and geometric configurations, facilitating faster reaction kinetics and enhancing selectivity by minimizing undesirable side reactions. SAMs thus act as precision nanomaterials, promising significant efficiency enhancements in energy systems, such as Li–S batteries and metal–air batteries.[81,82]

One remarkable advantage of SAMs lies in their high atom utilization efficiency, a feature derived from their atomic-scale design.[83,84] Unlike conventional catalysts, SAMs maximize the use of each atom for electrochemical reactions, crucial for resource sustainability and cost-effectiveness. By ensuring minimal waste and homogeneous distribution of active sites, SAMs enhance catalytic effectiveness while aligning with principles of green chemistry.[41,85] This efficiency fosters sustainable energy systems. Furthermore, SAMs offer potential economic feasibility owing to several inherent factors in their design and synthesis.[86] They require fewer raw materials compared to traditional bulk catalysts, thanks to precise atom placement that enhances precursor utilization. This reduction in precursor usage contributes directly to the economic viability of the synthesis process.

### 2.2. Operation Mechanism of SAMs

SAMs have demonstrated remarkable potential in revolutionizing energy storage technologies, pivotal in improving efficiency and durability (Figure 1). This section explores SAMs' specific working mechanisms in three key applications: metal-ion batteries, metal–sulfur batteries, and metal–air batteries.

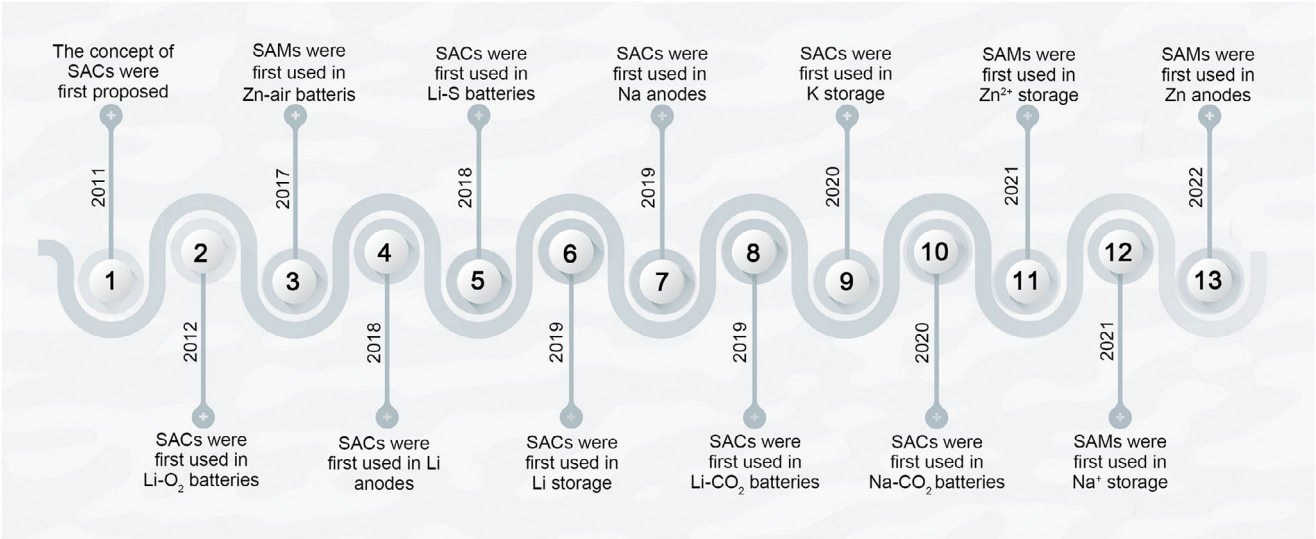


**Figure 2.** Timeline of single-atom materials used in the energy storage systems.

In metal-ion batteries, SAMs alter the electrode's electronic structure,[87] enhancing charge transfer kinetics and minimizing side reactions.[88] The precise control over active sites facilitates optimized redox reactions, resulting in higher energy density and prolonged cycle life. The introduction of isolated metal atoms induces changes in the electronic environment, leading to improved conductivity and electrochemical performance.[89] This precision control at the atomic level enhances charge transfer kinetics during metal ions intercalation and deintercalation, promoting a consistent and controlled environment for metal-ion storage. The atomic-level precision of SAMs minimizes the formation of unwanted side products and improves the reversibility of electrochemical reactions. Consequently, SAMs contribute to increasing energy density and cycle life, crucial factors for the practical applications of metal-ion batteries. They suppress side reactions through electronic structure modification, ensuring electrode stability and reducing parasitic reactions. SAMs also act as efficient catalytic centers, enhancing de-solvation and metal-ion transport kinetics, while promoting a more uniform distribution of metal ions within the electrode, thus minimizing capacity loss during cycling.

SAMs optimize metal–sulfur batteries by ameliorating sulfur's poor conductivity and polysulfide shuttle effect.[68,70,90] Through tailored electronic structures, SAMs reduce the reaction activation energy, accelerating conversion kinetics, while isolated metal atoms serve as catalytic centers, facilitating polysulfides conversion to stable lithium sulfides. This dual action enhances the battery's rate capability and longevity by curbing capacity fading. The polysulfide shuttle effect, a notorious problem in Li–S batteries, is mitigated by SAMs due to their atomically dispersed active sites, which exhibit strong binding affinity for polysulfides. By immobilizing polysulfides, SAMs prevent their migration between the cathode and anode, thereby contributing to enhanced cycling stability and reduced capacity fading over multiple charge–discharge cycles. Furthermore, SAMs facilitate sulfur conversion reactions by serving as catalytic centers, optimizing charge redistribution and activation energy barriers during the process. Atomically dispersed metal sites on the cathode surface facilitate uniform charge distribution, enhance sulfur utilization efficiency, and thereby lead to improved areal and volumetric capacities in metal–sulfur batteries. This optimized charge redistribution not only enhances the overall efficiency of sulfur conversion reactions but also mitigates issues related to uneven electrode utilization. In addition to catalyzing sulfur conversion reactions, SAMs contribute to improved electrode stability by accommodating large volume changes inherent in sulfur conversion reactions. Their atomically dispersed nature ensures uniform stress distribution, thus reducing mechanical strain on the electrode material and mitigating electrode degradation and pulverization issues over the battery's lifespan.

The function of SAMs in metal–air batteries centers on their ability to expedite oxygen reduction and carbon dioxide reduction reactions.[91,92] Through local electronic environment alterations, SAMs diminish the activation energy required for these reactions, thereby enhancing catalytic activity at the electrode–electrolyte interface, resulting in improved overall battery performance. SAMs exhibit high atom utilization efficiency, ensuring significant contribution of each metal atom to catalytic activity, thereby minimizing waste and bolstering the sustainability of metal–air battery systems. With their atomically dispersed active sites, SAMs significantly enhance the efficiency of the ORR at the cathode, optimizing oxygen molecule adsorption and activation while reducing associated overpotential. This catalytic enhancement translates to improved cathodic performance, elevating energy conversion efficiency in metal–air batteries. In metal–air batteries, the $CO_2$RR competes with the ORR at the cathode, affecting overall battery performance. SAMs play a crucial role in promoting the selective reduction of oxygen over carbon dioxide. Atomically dispersed metal sites act as catalytic centers, promoting oxygen conversion to hydroxide ions while suppressing undesired side reactions related to the $CO_2$RR, thus enhancing battery stability and efficiency. SAMs also optimize charge transfer kinetics during both ORR and $CO_2$RR processes. Atomically dispersed metal atoms act as efficient charge transfer mediators,

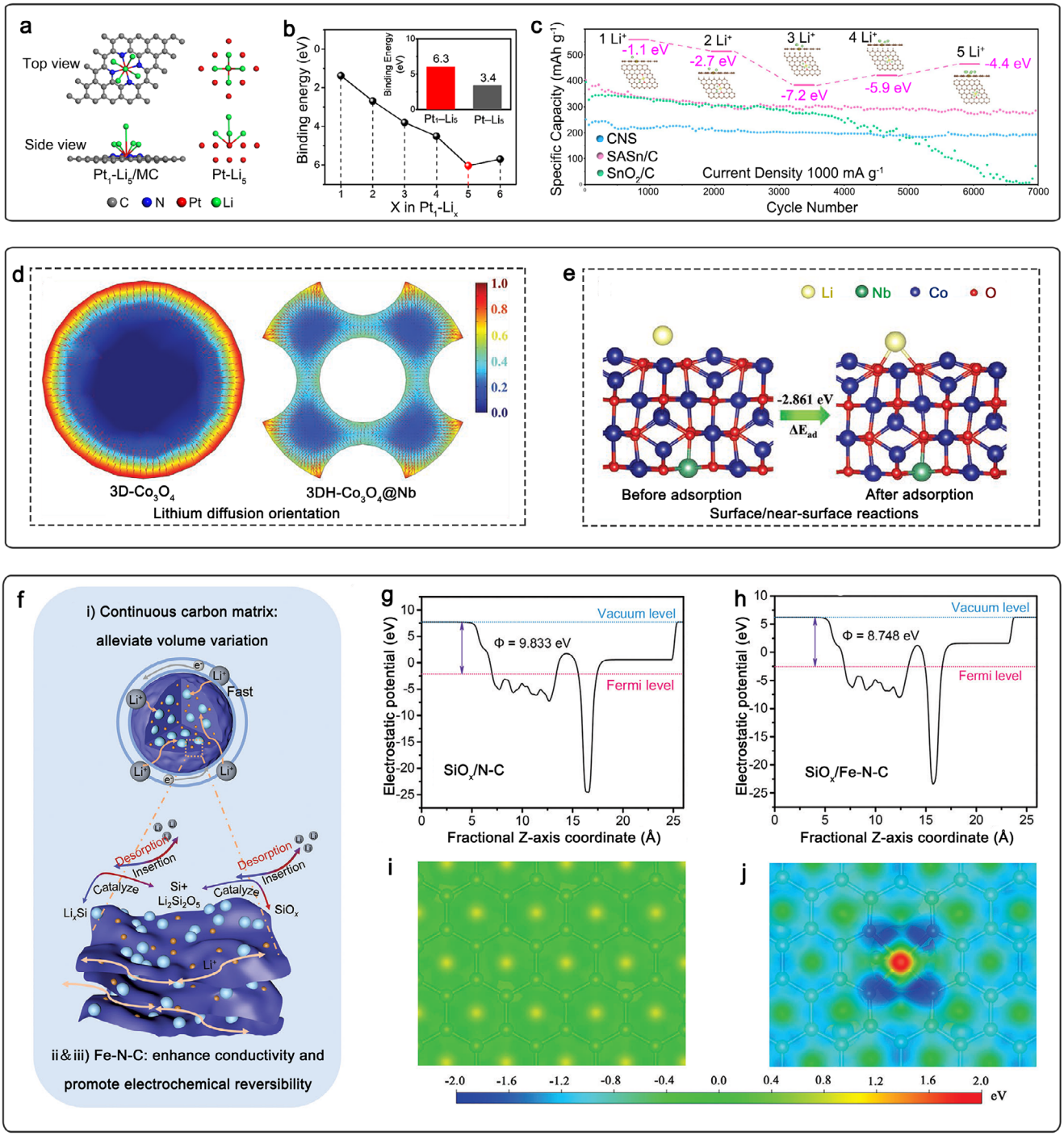


**Figure 3.** a) Optimized geometrical structures for the atomic $Pt_1$-$Li_5$ and bulk Pt-$Li_5$. b) Binding energies for the $Pt_1$-$Li_x$/MC. The inset shows the binding energies for the atomic $Pt_1$-$Li_5$ and bulk Pt-$Li_5$. Reproduced with permission.[89] Copyright 2019, by American Chemical Society. c) Ultralong-term cycling performance for CNS, SASn/C, and $SnO_2$/C at 1000 mA $g^{-1}$ and adsorption energy versus adsorption number of $Li^+$ on the single atomic Sn-doped carbon. The brown, red, yellow, and green spheres represent C, O, Sn, and Li atoms, respectively. Reproduced with permission.[102] Copyright 2022, Elsevier Ltd. d) Different lithium diffusion orientation in 3D-$Co_3O_4$ and 3DH-$Co_3O_4$@Nb. e) Adsorption configurations of Li on the 3DH-$Co_3O_4$@Nb surface. Reproduced with permission.[106] Copyright 2022, Wiley-VCH. f) Schematic illustration of the reversible conversion-alloy reaction for boosted lithium storage performance of $SiO_x$/Fe-N-C during the discharging/charging processes. The work functions for g) $SiO_x$/N-C and h) $SiO_x$/Fe-N-C, respectively. The calculated electron-density isosurface for i) $SiO_x$/N-C and j) $SiO_x$/Fe-N-C, respectively. The electron-density isosurface was plotted at 0.01 e $bohr^{-3}$. The color bar represented the electrostatic potential scale. Reproduced with permission.[87] Copyright 2022, Wiley-VCH.

facilitating electron movement between the electrode and reaction sites, thereby ensuring rapid electrochemical reactions and improved battery performance, especially in terms of power density and rate capability. The deleterious cathode degradation observed in metal–air batteries, commonly linked to the accumulation of reaction by-products, finds effective mitigation in the presence of SAMs. SAMs featuring atomically dispersed active sites act as favorable sites for the adsorption and decomposition of reaction intermediates, effectively preventing their buildup on the cathode surface. This function markedly enhances cycling stability and prolongs the overall lifespan of metal–air batteries.

The working mechanisms of SAMs in metal-ion, metal–sulfur, and metal–air batteries hinge on their adeptness at altering electronic structures, diminishing reaction activation energies, and expediting dynamic processes. These mechanisms collectively contribute to the enhanced efficiency, durability, and sustainability of energy storage systems.

### 2.3. Challenges of SAMs

The stability and durability of SAMs pose significant challenges critical for their effective integration into energy storage systems.[53,93] While SAMs exhibit remarkable electrochemical activity, prolonged cycling exposes them to environmental conditions and reactants, presenting hurdles to their longevity. Typically comprising active metal atoms coordinated within a matrix or support material, SAMs' high chemical reactivity can lead to undesirable interactions with the surroundings, potentially degrading sites and reducing electrochemical activity over time. Extended cycling and exposure to reactive species may induce structural changes in both the support material and SAMs' atomic configuration, altering their electronic and geometric properties and affecting performance. SAMs may also be sensitive to environmental factors like temperature, humidity, and gas composition, which can alter the chemical state of metal atoms and impact stability. Repeated cycling imposes mechanical stress on SAMs and their support matrix, potentially causing deterioration. Additionally, exposure to unfavorable reaction intermediates, such as reactive radicals or corrosive species, can accelerate degradation, compromising long-term stability. Tackling these challenges necessitates a thorough comprehension of SAMs' behavior under real-world operating conditions.[73,94] Robust strategies for stabilizing single-atom sites and mitigating external influences are crucial for realizing SAMs' full potential in energy storage technologies.

## 3. Metal-Ion Batteries and Supercapacitors

### 3.1. Metal-Ion Batteries

Metal-ion batteries, including LIBs, SIBs, PIBs, and ZIBs, play a pivotal role in energy storage across various devices. Among them, LIBs have found extensive use in portable electronic devices, electric vehicles, and energy storage stations.[95–101] However, the graphite anode in commercial use faces limitations due to its limited theoretical capacity (372 mAh $g^{-1}$) and slow $Li^+$ diffusion. To enhance carbon-based materials' electrochemical performance in LIBs, researchers have introduced single metal atoms with lithium-storage activity, such as Pt,[89] Sn,[102] Au,[103] and Ag,[103] onto carbon-based materials. For instance, Wang and co-workers developed atomic Pt loaded carbon-based material ($Pt_1$/MC) through a modified photochemical solid-phase reduction method.[89] Pt single atoms interact with Li atoms, forming a Pt–Li alloy, significantly boosting lithium storage capacity (**Figure 3a**). Density functional theory (DFT) calculations confirm Pt atoms' ability to anchor Li ions on the carbon substrate (Figure 3b).[89] Consequently, $Pt_1$/MC exhibits exceptional electrochemical performance, achieving a capacity of 846 mA h $g^{-1}$ after 800 cycles at 2 A $g^{-1}$ and retaining 349 mA h $g^{-1}$ after 6000 cycles at 5 A $g^{-1}$. (**Table 1**).[89] Similarly, the incorporation of other metals (Au, Ag, and Sn) with lithium-storage activity in porous carbon-based materials exhibits promising electrochemical performance (Table 1).[103] Unlike noble metals, a single Sn atom coordinates with two O and two C atoms in the carbon matrix, forming Sn—O—C and Sn—C bonds.[102] This unique coordination facilitates efficient electron and ion transfer, boosting electrochemical kinetics. For example, a single atom Sn/C anode exhibits a minimal capacity degradation rate of 0.0031% per cycle at 1000 mA $g^{-1}$ after 7000 cycles (Table 1 and Figure 3c). Additionally, DFT calculations illustrate that Sn atoms can adsorb three $Li^+$ when fully discharged (Figure 3c).[102] During charging, $Li^+$ ions are released directly from Sn atoms rather than through the typical dealloying pathway, offering improved structural stability and enhanced rate performance in carbon-based electrodes.

**Table 1.** Electrochemical performance of single-atom materials in LIBs.

| Materials | Current density [A $g^{-1}$] | Specific capacity [mAh $g^{-1}$] | Cycles | Ref. |
|---|---|---|---|---|
| $Pt_1$/MC | 2 | 846 | 800 | [89] |
| | 5 | 349 | 6000 | |
| $Ag_{SA}$-porous carbon | 1.68 | ≈340 | 200 | [103] |
| $Pt_{SA}$-porous carbon | 1.68 | ≈275 | 200 | |
| $Au_{SA}$-porous carbon | 1.68 | ≈125 | 200 | |
| SASn/C | 1 | 281 | 7000 | [102] |
| 3DH-$Co_3O_4$@Nb | 5 | 740 | 1000 | [106] |
| Co-N-C | 1.86 | 1000 | 800 | [105] |
| Co-CN | 2 | 589.1 | 900 | [104] |
| $SiO_x$/Fe-N-C | 0.1 | 799.1 | 100 | [87] |
| | 5 | 173.7 | 5000 | |

Regarding single-atom metals without lithium-storage activity, such as Co,[104,105] Fe,[87] and Nb.[106] their presence significantly enhances electrochemical performance by improving electron conductivity and accelerating surface/near-surface reactions, leading to enhanced pseudocapacitance behavior and improved rate capabilities. For example, Yin et al. introduced a single-atom Nb-based composite material (3DH-$Co_3O_4$@Nb), which exhibits an interconnected 3D hierarchically porous structure, enhancing the availability of active surface areas (Figure 3d).[106] The presence of Nb atoms enhances lithium absorption capacity compared to the $Co_3O_4$ substrate (Figure 3e). 3DH-$Co_3O_4$@Nb maintains a reversible capacity of ≈740 mA h $g^{-1}$ even after 1000 cycles under 5 A $g^{-1}$ (Table 1).[106] Additionally, introducing Co single atoms into porous carbon (Co—N—C)[104] and

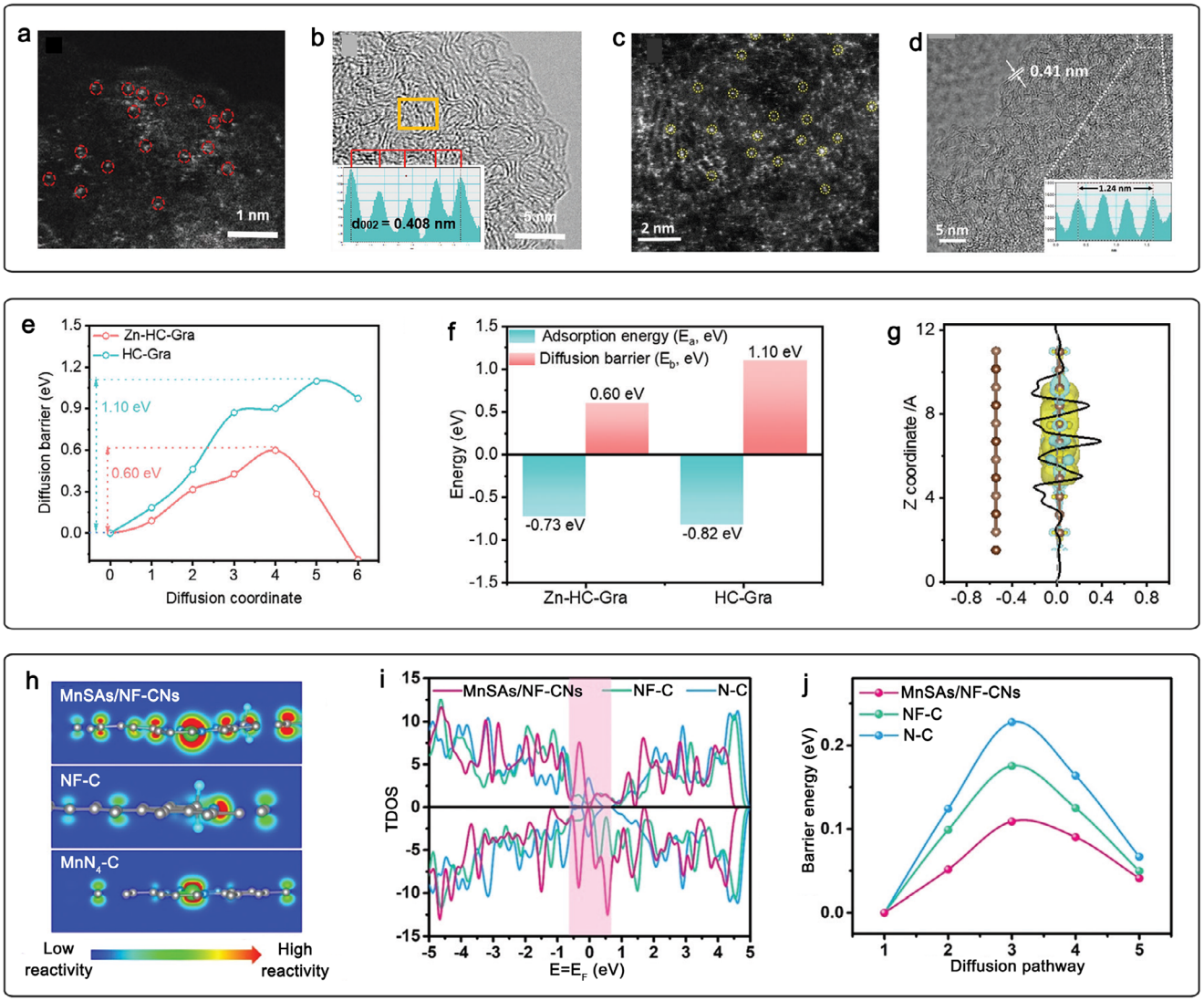


**Figure 4.** a) HAADF-STEM image and b) HRTEM image of Zn-HC. Reproduced with permission.[110] Copyright 2023, Wiley-VCH. c) HAADF-STEM image and d) HRTEM image of MnSAs/NF-CNs. Reproduced with permission.[111] Copyright 2021, Royal Society of Chemistry. e) Diffusion barrier energies and f) adsorption energy for Zn-HC-Gra and HC-Gra, respectively. g) Isosurface of charge density difference and planar-average charge density plot of Zn-HC-Gra. Reproduced with permission.[110] Copyright 2023, Wiley-VCH. h) The corresponding sectional reactivity heat map for the active sites of the MnSAs/NF-CNs, NF-C, and $MnN_4$-C, where the red and blue colors indicate the higher and lower reactivity, respectively. i) The density of states of different carbon structures and j) the corresponding barrier energy.[111] Reproduced with permission. Copyright 2021, Royal Society of Chemistry.

g-$C_3N_4$ (Co-CN)[105] enhances Li ion transportation and storage. Nevertheless, carbon-based materials have yet to surpass inherent theoretical limitations. Therefore, alternative single atoms should be considered for achieving high lithium storage capacity. Researchers have discovered that introducing single atoms into host materials can significantly enhance electrical conductivity. Building upon this, the integration of atomically dispersed metals can enhance the electric conductivity of carbon-based materials and benefit low-electric-conductivity materials, such as $SiO_x$ nanoparticles. Pang and co-workers introduced $SiO_x$/Fe—N—C material through straightforward electrospray-carbonization.[87] When employed as a LIB anode, $SiO_x$/Fe—N—C exhibits remarkable improvements in discharge capacity, enhanced rate capabilities (Figure 3f), and good long-term stability (Table 1), surpassing $SiO_x$/N—C and $SiO_x$ counterparts.[87] This improvement is attributed to reduced work function, which accelerating electron transfer (Figure 3g and 4h), as supported by electron-density isosurface calculations (Figure 3i and 4j).

Owing to the limited availability of lithium resources, attention has shifted toward sodium-based energy storage systems, prompting the development of SIBs. However, SIBs encounter challenges akin to those of LIBs, such as restricted metal-ion diffusion and slow reaction kinetics, which impede their large-scale deployment. Notably, $Na^+$ presents a larger ionic radius than $Li^+$, exacerbating issues such as substantial volumetric variation and sluggish $Na^+$ diffusion.[107–109] For instance, while carbon-based materials excel in storing lithium in LIBs, they demonstrate

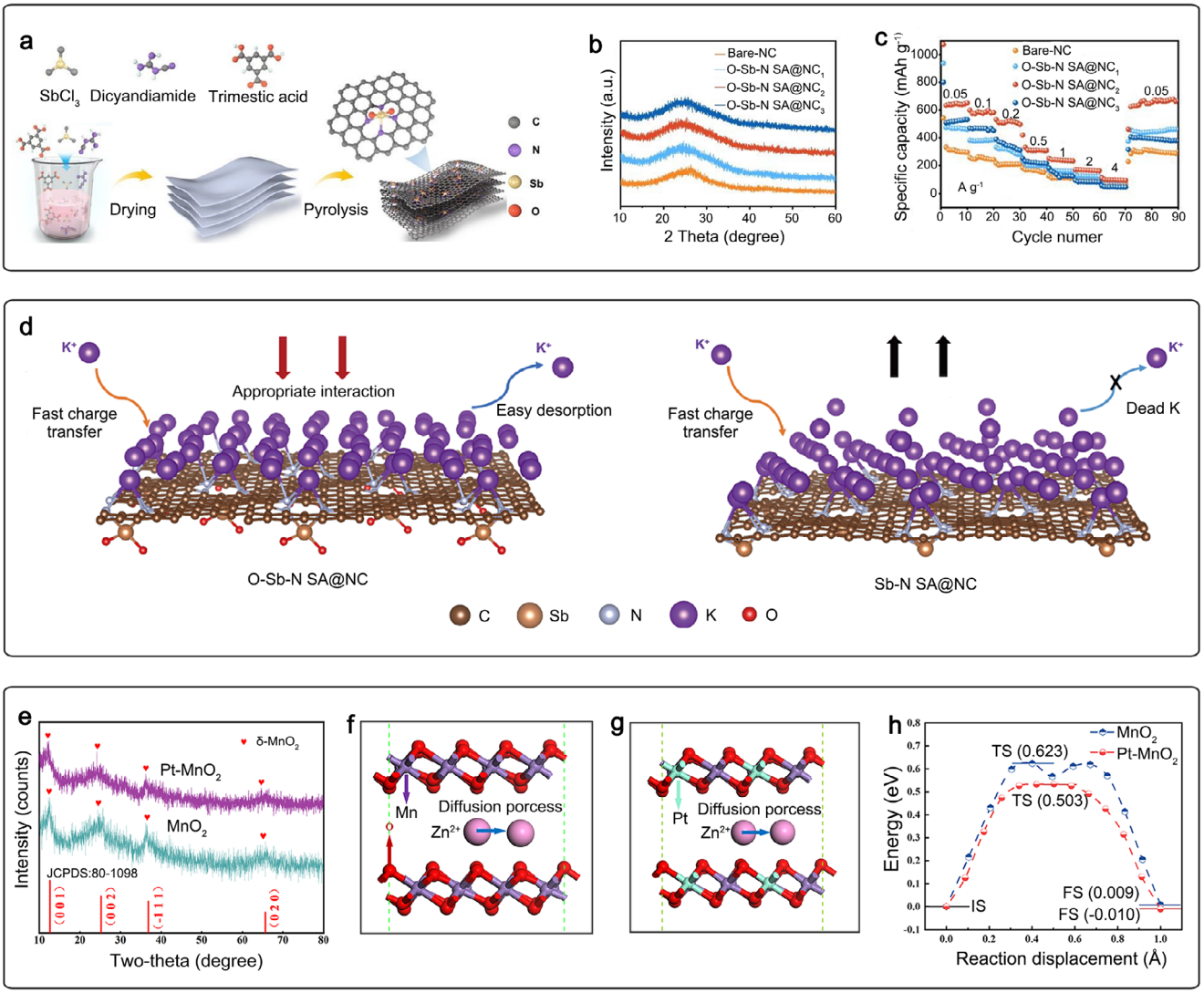


**Figure 5.** a) Schematic diagram of the synthesis process of O-Sb-N SA@NCs. b) XRD patterns of Bare-NC and O-Sb-N SA@NCs. c) Rate performances of all samples at various current densities. d) Schematic illustration of $K^+$ adsorption and desorption on the Sb-N SA@NC and Sb-N SA@NC, respectively. Reproduced with permission.[114] Copyright 2023, Royal Society of Chemistry. e) XRD patterns of Pt-$MnO_2$ and $MnO_2$. Zinc-ion diffusion model of f) $MnO_2$ and g) Pt-$MnO_2$. h) Calculated zinc-ion diffusion energy barriers of Pt-$MnO_2$ and $MnO_2$. Reproduced with permission.[123] Copyright 2021, by American Chemical Society.

significantly lower sodium storage capacities in SIBs. To tackle this limitation, researchers are exploring methods to expand the interlayer space of carbon-based materials, creating ample room for sodium storage. One effective approach involves immobilizing single metal atoms within the carbon matrix. For instance, Zhao and co-workers adopted a high-temperature pyrolysis strategy to incorporate single-atom Zn into hard carbon materials (Zn–HC), significantly increasing the interlayer space by up to 0.408 nm (Figure 4a and 5b).[110] Similar enhancements have been observed with single-atom Mn[111] and Cr.[112] Single-atom Mn can expand the interlayer space by up to 0.41 nm, surpassing graphite's typical value of 0.335 nm (Figure 4c and 5d).[111] Similarly, incorporating Cr single atoms shifts the (002) peak associated with graphite interlayer to a lower angle, indicating increased spacing.[112] The expanded interlayer spacing offers promising prospects for sodium storage and contributes to the enhanced performance of carbon-based materials in SIBs. For instance, the Zn–HC anode shows a high reversible capacity of 305 mAh $g^{-1}$ at 2 A $g^{-1}$ after 3800 cycles, as well as a substantial capacity retention of 443 mAh $g^{-1}$ at a low temperature of −40 °C (**Table 2**). The inclusion of Zn single atoms significantly enlarges the carbon interlayers and reduces the diffusion barrier for $Na^+$ (Figures 4e and 5f). Additionally, the isosurface of charge density difference suggests that the introduction of Zn atoms enhances the electron state, thereby expediting electron transfer (Figure 4g). Similarly, the incorporation of Mn single atoms provides additional active sites, improves electrical conductivity, and reduces the diffusion barrier of $Na^+$ (Figures 4h and 5j), thus improving the electrochemical performance of the anode material. Notably, the MnSAs/NF-CNs

**Table 2.** Electrochemical performance of single-atom materials in SIBs.

| Materials | Current density [A $g^{-1}$] | Specific capacity [mAh $g^{-1}$] | Cycles | Ref. |
|---|---|---|---|---|
| Zn-HC | 2 | ≈270 | 5000 | [110] |
| | 2 | ≈305 | 3800 | |
| CrSAs/NPC | 1 | ≈190 | 100 | [112] |
| Zn–$N_3$S–NSC | 1 | ≈80 | 1000 | [239] |
| | 0.2 | ≈160 | 4000 | |
| MnSAs/NF-CNs | 5 | ≈220 | 7000 | [111] |
| $Fe_3$N@N-3DPCN | 5 | ≈200 | 5000 | [240] |

enable exceptional specific capacity (≈220 mAh $g^{-1}$) with an ultralong cycling life up to 7000 cycles,[111] surpassing reported performance metrics for SAMs in SIBs (Table 2).

Different from LIBs and SIBs, PIBs have garnered considerable attention due to the abundant availability of the K element and its low redox potential. Nevertheless, similar to SIBs, PIBs also encounter challenges associated with significant volume changes due to the larger ionic radius of potassium ions.[40,61,113] For instance, graphite can form $KC_8$ intercalation compounds with potassium, offering a capacity of ≈280 mAh $g^{-1}$ but suffering from substantial volume expansion exceeding 70%, leading to rapid capacity decay. Inspired by strategies used in SIBs, introducing single-atom metals to carbon-based materials proves effective in mitigating these challenges in PIBs. For instance, Zhang et al. synthesized single-atom antimony (Sb) dispersed nitrogen-doped porous carbon nanosheets (O–Sb–N SA@NC) via a high-temperature pyrolysis method (Figure 5a).[114] Their observation revealed that after introducing single-atom Sb, the (002) reflection peak shifted to lower angles, in contrast to pure nitrogen-doped carbon (Figure 5b). This indicates that Sb atoms expand the interlayer spacing of carbon, providing ample room for potassium storage. A similar phenomenon has also been observed in the MnSAs/NF-CNs materials.[111] Besides, Sb atoms can react with K atoms, forming a $K_xSb$ alloy, thereby providing additional K storage capacity. Consequently, the O-Sb-N SA@NC anode exhibits remarkable performance in terms of substantial reversible capacities (593.3 mAh $g^{-1}$, 100 cycles at 0.1 A $g^{-1}$), excellent rate capability, and prolonged durability for PIBs (Figure 5c and **Table 3**). The O–Sb–N coordination sites enhance the K ions storage capability and significantly reduce the volume change (Figure 5d). Alongside single-atom Sb, other single-atom metals with K-reactive activity, such as Zn[115] and Te,[116] accelerate the adsorption/desorption of K ions. For instance, Wu and co-workers delivered a facile template method to introduce high-loading (12 wt.%) Zn single atoms into hollow carbon spheres (Zn-N-S@C), enhancing long cyclic life for potassium storage (Table 3).[115] Furthermore, Te@N,P-codoped PCNFs, composed of Te single atoms embedded in N,P-co-doped porous carbon nanofibers, demonstrate strong adsorption capabilities enhanced by heteroatoms co-doping in the carbon matrix.[116] This unique structure enables a high reversible capacity, with a value of 323.7 mAh $g^{-1}$ after 700 cycles at 0.5 C (Table 3).[116] Even single atoms lacking K-reactive activity, such as Ni atoms, contribute to enhancing electrochemical performance for K storage.[88,117] For instance, Qian et al. incorporated single-atom Ni into S/C nanotubes, resulting in a high potassium storage capacity of 330.6 mAh $g^{-1}$ at 1000 mA $g^{-1}$ after 500 cycles (Table 3).[88] Besides, the introduction of Ni atoms into B and N co-doped hard carbon nanotubes has led to a remarkably high reversible capacity of 694 mAh $g^{-1}$ at 0.05 A $g^{-1}$ (Table 3). The edge sites of Ni-$N_4$-B serve as active sites for the interlayer adsorption of potassium ions, while the presence of Ni atoms enhances the reversibility of potassium storage on nitrogen and boron atoms.[117] This enhancement can be credited to the uniformly distributed Ni species at the atomic level, which improves the conversion kinetics and lowers the energy barrier for $K^+$ absorption.

Moving beyond carbon-based SAMs for potassium storage, researchers have explored alternative substrates, especially 2D MXenes, to exploit the distinctive advantages of single-atom catalysts, offering a transformative boost to the electrochemical performance of PIBs. Notably, a MXene-based aerogel adorned with single-atom Sb (Sb/$Ti_3C_2T_x$) showcased a remarkable capacity of 521 mAh $g^{-1}$ at 0.1 A $g^{-1}$ and maintained outstanding capacity retention of 94% at 1 A $g^{-1}$ even after 1000 cycles (Table 3).[118] This exceptional performance stems from the strategic integration of atomically dispersed Sb into the $Ti_3C_2T_x$-MXene layers, inducing profound modifications in the electronic structure of MXene, thus elevating its electrochemical performance.[118] Furthermore, the integration of single-atom metals into MXene layers enhances K storage capabilities at heterointerfaces. These findings herald a promising single-atom engineering approach for the rational design of high-performance electrode materials in PIBs, charting a path for future advancements in this dynamic field.

Aqueous rechargeable ZIBs hold immense promise for large-scale energy storage, boasting high safety, low cost, and environmental friendliness.[119–122] Unlike LIBs, SIBs, and PIBs, ZIBs operate through a two-electron transfer process, suggesting higher energy density potential. However, the diffusion of zinc ions is hindered by the electrostatic effects of bulky $Zn^{2+}$, resulting in poor rate performance. To tackle this challenge, Li et al. investigated the integration of single-atom Pt as active sites in $MnO_2$ to enhance zinc ion diffusion.[123] They synthesized a Pt-$MnO_2$ nanocomposite cathode material for ZIBs by depositing single-atom Pt onto $MnO_2$ using thermostatic electrochemical deposition (Figure 5e). The resulting Pt-$MnO_2$

**Table 3.** Electrochemical performance of single-atom materials in PIBs.

| Materials | Current density [A $g^{-1}$] | Specific capacity [mAh $g^{-1}$] | Cycles | Ref. |
|---|---|---|---|---|
| Ni/S/C nanotubes | 1 | 330.6 | 1000 | [88] |
| Zn-N-S@C | 2 | ≈140 | 4000 | [115] |
| | 0.1 | ≈350 | 200 | |
| Ni-$N_4$-B | 1 | ≈220 | 1500 | [117] |
| O-Sb-N SA@NC | 2 | ≈200 | 1000 | [114] |
| Te@N,P-codoped | ≈2.1 | ≈160 | 1500 | [116] |
| PCNFs | ≈0.2 | 323.7 | 700 | |
| Sb/$Ti_3C_2T_x$ | 1 | ≈300 | 1000 | [118] |
| | 0.1 | 521 | 100 | |

**Table 4.** Electrochemical performance of single-atom materials in supercapacitors.

| Materials | Current density [A $g^{-1}$] | Specific capacity [F $g^{-1}$] | Ref. |
|---|---|---|---|
| Ni–Co, N-$Mo_2C$ | 1 | 1004.8 | [129] |
| AC-Mn-3 | 1 | 516.2 | [132] |
| MnSAs/NMC | 0.5 | 444 | [128] |
| Mn-CNT | 1 | 1523.6 | [131] |
| $NiMoO_4$ nanorods | 2 | 122 | [124] |
| PCNM-Zn | 2 | 182.3 Wh $kg^{-1}$ | [127] |
| Zn/N-loading carbon materials | 0.1 | 621 | [126] |
| Pt-$MnO_2$ | 0.8 | 264 mA h $g^{-1}$ | [123] |
| Ag-decorated $MnO_2$ | 0.3 | 297.5 | [125] |
| Ni-1.0@N@HCN-Ar | 1 | 777 | [130] |

composite demonstrated impressive rate capabilities, maintaining a capacity of 264 mAh $g^{-1}$ at 800 mA $g^{-1}$. Their investigations revealed that introducing individual Pt atoms enhances electron conductivity by leveraging the low occupancy of the Pt 5d orbital. This also lowers the diffusion barrier of $Zn^{2+}$ during charge/discharge cycles (Figure 5f and 6h). Additionally, the synergistic interaction between diverse metals and the support promotes zinc ion diffusion. These findings highlight the beneficial role of single-atom Pt doping in enhancing the electrochemical properties of $MnO_2$ in ZIBs.[123]

### 3.2. Supercapacitors

Supercapacitors have attracted significant attention due to their high power density, rapid charge–discharge capability, and long cycle life, making them promising candidates for renewable energy storage, portable electronics, and electric vehicles.[124,125,123] However, traditional carbon-based electrode materials suffer from limited energy density and insufficient active sites, hindering their ability to meet the growing demands for high-performance energy storage.[126–128] Single-atom materials have emerged as a novel strategy to enhance electrode performance owing to their ≈100% atomic utilization, unique electronic structures, and tunable coordination environments.[129,130] By anchoring transition metal atoms in single-atom form onto carbon-based supports, SAMs can significantly improve pseudocapacitance contributions, charge transfer efficiency, and redox reaction kinetics.[131,132] This section summarizes recent advances in SAMs design and application in supercapacitors based on the previous studies (**Table 4**).

Lee et al. developed Ni-Co dual single-atom catalysts (NiCo-SADs) anchored on nitrogen-doped molybdenum carbide (N-$Mo_2C$) by in situ encapsulation of Ni-Co within molybdenum polydopamine and nitrogen doping (Figure 6a). The synergistic effect of the dual atoms optimized $OH^-$ adsorption energy, leading to a high specific capacitance of 1004.8 F $g^{-1}$ at 1 A $g^{-1}$ and 93.6% capacitance retention over 5000 cycles (Table 4 and Figure 6b).[129] DFT calculations revealed that Ni-Co dual-atom bridge sites substantially reduced the reaction energy barrier, facilitating rapid pseudocapacitive behavior. The assembled asymmetric supercapacitor achieved an energy density of 69.69 Wh $kg^{-1}$ at a power density of 8200 W $kg^{-1}$, providing a new approach for solid-state energy storage devices.[129] Wang et al. reported a $MnCl_2$ template-assisted synthesis of atomically dispersed Mn single atoms embedded in N-doped mesoporous graphite carbon (MnSAs/NMC) (Figure 6c,d). This material exhibited excellent pseudocapacitive performance of 444 F $g^{-1}$ at 0.5 A $g^{-1}$ (Table 4).[128] The large mesoporous surface area (1967 $m^2$ $g^{-1}$) combined with $MnN_2C_2$ active sites synergistically enhanced ion diffusion and electron transport (Figure 6e,g).[128] Besides, the authors proposed an innovative hybrid discharge mode combining zinc–air battery and supercapacitor characteristics, achieving a high energy density of 120.1 Wh $kg^{-1}$ along with instantaneous high power output, overcoming traditional device limitations. DFT analysis further elucidated the optimized $OH^-$ adsorption mechanism enabled by Mn single atoms.[128] Wen and his co-workers incorporated Mn single atoms into carbon nanotubes (Mn-CNT) via Mn–N coordination, significantly improving the electrode's specific capacitance to 1523.6 F $g^{-1}$ at 1 A $g^{-1}$ and an energy density of 180.8 Wh $kg^{-1}$ (Figure 6h).[131] The design utilized Ni-catalyzed CNT growth combined with highly polar Mn single-atom active sites to accelerate $OH^-$ adsorption and redox kinetics. The asymmetric supercapacitor maintained over 93.7% capacity retention after 7000 cycles and successfully powered an LED for 60 min, demonstrating promising practical application potential.[131] The study confirmed that strong interactions between single atoms and carbon supports effectively suppressed metal aggregation and extended device lifetime.

These recent advances demonstrate that precise single-atom catalyst design can substantially enhance supercapacitor energy density, rate performance, and cycling stability. Future research directions include developing versatile SAC synthesis methods to realize multi-metal synergy and diverse supports, in-depth investigation of dynamic interfacial reactions between single-atom sites and electrolytes, and promoting flexible and miniaturized device integration to meet diverse application needs. Single-atom materials provide a crucial technological pathway for next-generation high-performance supercapacitors, and their interdisciplinary development will accelerate innovation in energy storage technologies.

## 4. Metal Anodes

Lithium metal is considered as a highly promising anode for next-generation lithium-based batteries due to its high theoretical capacity (3860 mAh $g^{-1}$) as well as low redox potential (−3.04 V vs standard hydrogen electrode).[85,133,134] However, the practical application of rechargeable lithium metal batteries (LMBs) grapples with the persistent menace of dendrite formation on the lithium anode. These dendrites inflict reduced Coulombic efficiency (CE), heightened charge/discharge overpotentials, and a curtailed cycling life.[135–137] Furthermore, the expansion of dendritic lithium raises grave safety concerns, including the specter of internal short circuits, thermal runaway, and potentially life-threatening accidents. To address these challenges, extensive research spanning decades has explored various strategic avenues. These strategies include modifying the lithiophilicity of substrates to foster uniform nucleation, engineering deposition

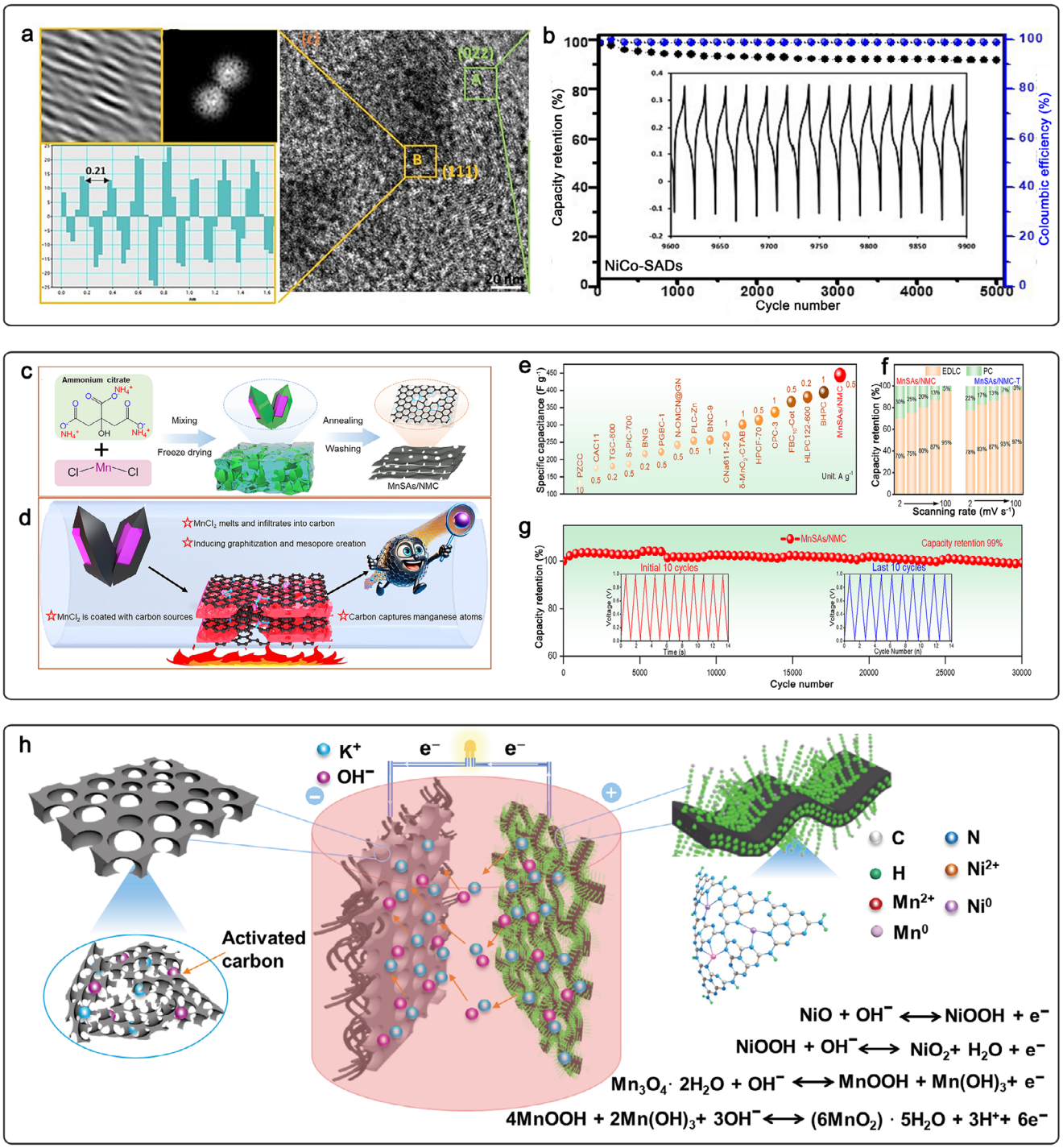


**Figure 6.** a) Structural and microscopic study of NiCo-SADs. b) Cycling stability of NiCo-SADs at 10 A $g^{-1}$. Reproduced with permission.[129] Copyright 2024, Elsevier Ltd. c) Synthetic diagram of MnSAs/NMC. d) Graphical representation of the MnSAs/NMC carbonation process. e) Comparison of the specific capacitance of MnSAs/NMC with other carbon electrodes in a three-electrode system. f) Contribution ratios of electric double-layer capacitance and pseudo-capacitance for MnSAs/NMC and MnSAs/NMC-T. g) Cycle stability for MnSAs/NMC-based symmetric supercapacitor at 5 A $g^{-1}$. Reproduced with permission.[128] Copyright 2024, Elsevier Ltd. h) Schematic illustration showing the reaction pathway of Mn-CNT@C asymmetric supercapacitor. Reproduced with permission.[131] Copyright 2024, Tsinghua University Press.

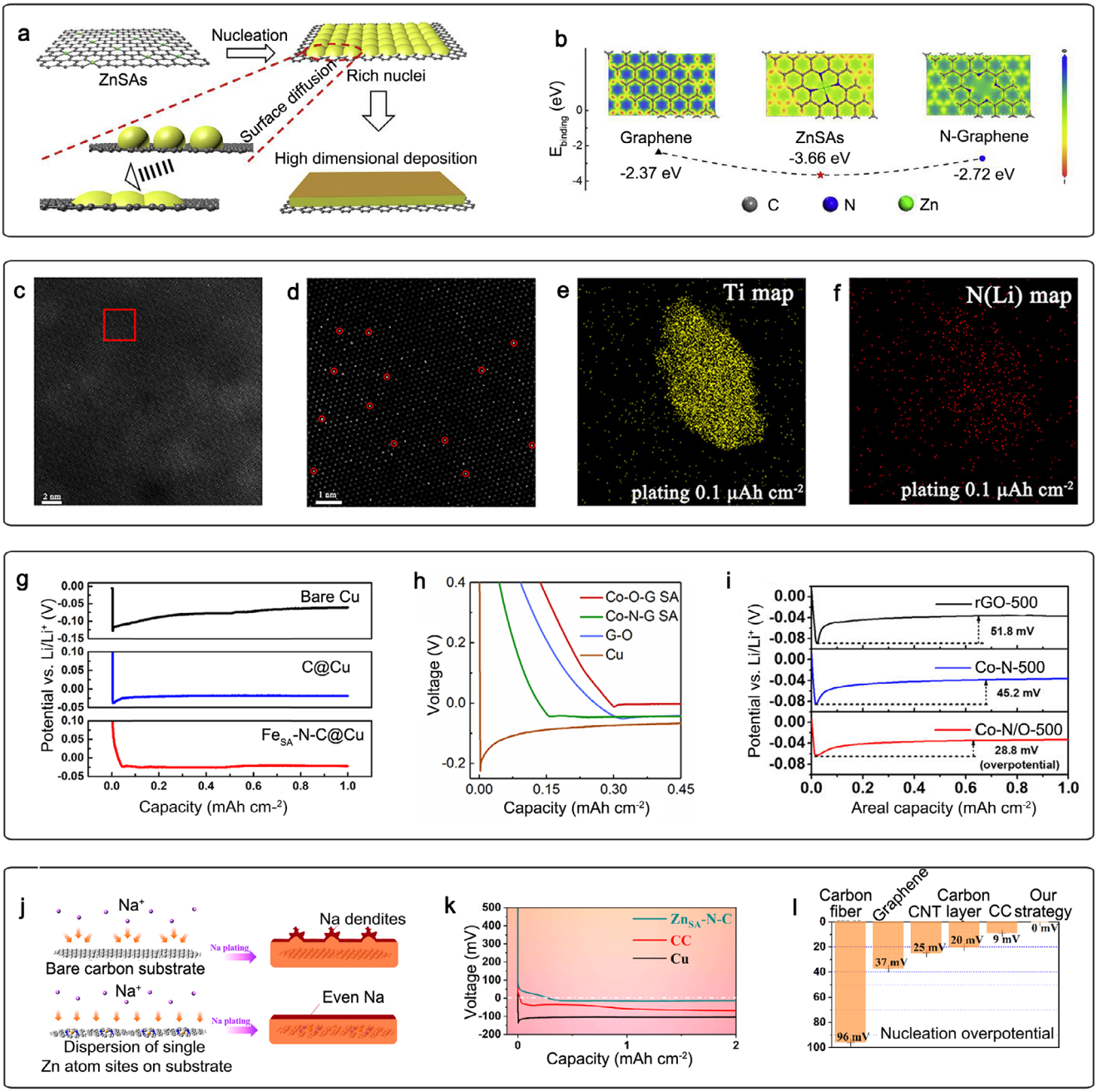


**Figure 7.** a) High-dimensional deposition on single-atom Zn sites. b) Electron density difference and surface binding energy of graphene, ZnSAs, and N-graphene. Reproduced with permission.[142] Copyright 2019, Elsevier Ltd. c) and d) HAADF-STEM images of a Zn-MXene nanosheet, showing the high-density bright dots (Zn atoms) on the MXene nanosheets. Element distribution of e) Ti and f) N (Li), which indicates a homogeneous nucleation of Li on Zn-MXene layers. Reproduced with permission.[82] Copyright 2020, by American Chemical Society. g) Overpotential of metallic Li plating on bare Cu, C@Cu, and FeSA-N-C@Cu electrodes. Reproduced with permission.[143] Copyright 2019, by American Chemical Society. h) Nucleation voltage profiles of Co-O-G SA, Co-N-G SA, G-O, and Cu electrodes at the first cycle. Reproduced with permission.[144] Copyright 2021, by Chinese Chemical Society. i) Nucleation overpotential at 1 mA cm$^{-2}$ of rGO-500, Co-N-500, and Co-N/O-500. Reproduced with permission.[145] Copyright 2022, Wiley-VCH. j) Schematic illustration of Na plating behavior on Zn$_{SA}$-N-C electrodes. k) Voltage profiles of galvanostatic Na deposition on different substrates. l) The nucleation overpotential of different substrates. Reproduced with permission.[84] Copyright 2019, by American Chemical Society.

**Table 5.** Electrochemical performance of single-atom materials in Li anode.

| Strategy | Materials | Nucleation overpotential [mV] | Current density [mA cm$^{-2}$] | Capacity [mAh cm$^{-2}$] | Cycle life [h] | Ref. |
|---|---|---|---|---|---|---|
| Substrate modification | $Zn_{SAs}$-graphene | / | 1 | 1 | 800 | [142] |
| | $Fe_{SA}$-N-C | 0.8 | 1 | 1 | 200 | [143] |
| | Co-O-G SA | 10.5 | 1 | 1 | 780 | [144] |
| | Co-N-G SA | 44.3 | 1 | 1 | 600 | |
| | Co-N | 45.2 | 1 | 1 | ≈900 | [145] |
| | Co-N/O | 28.8 | 1 | 1 | 2000 | |
| | Zn-MXene | 11.3 | 1 | 1 | 1200 | [82] |
| 3D hosts | $CoN_x$-doped graphene | 6 | 2 | 2 | ≈400 | [152] |
| | SAMn@NG | / | 1 | 1 | 560 | [155] |
| | NOMC-Ni | 31 | 5 | 4 | 1330 | [153] |
| | CC@CN-SACo | 12.3 | 2 | 1 | 1400 | [154] |
| | | | 1 | 1 | 2000 | |
| Protect layers | B/2D MOF-Co | 53 | 5 | 5 | 300 | [81] |
| | rGO@Ru SAs | / | 1 | 1 | 400 | [165] |
| | FeCoDA-CN@PP | / | 1 | 1 | 500 | [194] |
| | Co—$N_x$ | 22 | 3 | 3 | 1500 | [178] |
| | $Zn_1$-HNC | / | 3 | 3 | 1200 | [181] |
| | SACo/ADFS@HPSC | 15 | 0.5 | 0.5 | 1600 | [241] |
| | Mo/NG | / | 0.5 | 0.5 | 1000 | [166] |

hosts to confine electrode expansion/contraction during Li deposition/stripping, and tailoring the composition of electrolytes or incorporating additives to forge stable and functional protective layers.[93,138–141] These approaches have shown significant advancements in preventing and suppressing the formation of dendrites.

Recently, single-atom materials have garnered growing attention owing to their significantly elevated surface free energy. This characteristic endows them with exceptional properties, making them ideal nucleation sites for lithium deposition by facilitating higher reactivity and promoting uniform, multidimensional growth. Furthermore, SAMs can be densely loaded and exhibit superior homogeneity, providing an increased number of deposition sites and facilitating uniform nucleation on the electrode surface. Thus, researchers have integrated SAMs existing strategies, such as substrate modification, the implementation of 3D hosts, and the application of protective layers. This synergistic approach aims to actively inhibit the development of Li dendrites and elevate battery performance. Through the incorporation of SAMs into the design, the nucleation and deposition processes are finely controlled, leading to improved battery performance and bolstered safety standards.

### 4.1. Inducing Metal Nucleation on Substrate

Drawing from Cui research group's insights, metals with definite solubility in lithium experience minimal nucleation barriers, while those with negligible solubility face significant hurdles.[80] Considering the binary phase between metals and lithium, metals such as Zn, Au, and Ag, capable of dissolving in lithium, promote Li nucleation. Building upon this knowledge, lithiophilic metals facilitating effective Li nucleation have been integrated into lithium metal anodes, and single-atom metals are no exception to this trend. For example, Qian and co-workers fabricated single-atom Zn-loaded graphene nanomaterials via high-temperature pyrolysis of ZIF.[142] These single-atom Zn sites on graphene serve as lithium plating substrates, enhancing high-dimensional Li deposition kinetics and mitigating dendrite formation (**Figure 7a**). Subsequently, symmetric Li-$Zn_{SAs}$ cell measurements demonstrate steady voltage oscillations over 800 h, indicating improved stability (**Table 5**). The heightened surface energy of these zinc sites enhances Li atom binding and stability, while a lower migration barrier facilitates easier Li migration to neighboring areas rather than local aggregation (Figure 7b).[142] However, the nucleation and growth processes of lithium on SAMs are still unclear. Therefore, further investigation is needed to explore this aspect. Yang and co-workers adopted a molten-salt etching and anchoring method to prepare lithiophilic single-atom Zn dispersed $Ti_3C_2Cl_x$ layers.[82] The homogeneous dispersion of Zn atoms (Figure 7c,d), when used as the substrate for Li plating, ensures a uniform Li distribution on MXene layers (Figure 7e,f), leading to flat Li morphology on anodes. This Zn-MXene-Li system exhibits excellent stability, maintaining performance for up to 1200 h (Table 5).[82] This indicates that the fixation of individual lithiophilic zinc atoms on MXene layers serves as stable nucleation sites for lithium.[82] These findings suggest that the incorporation of lithiophilic single metal atoms on different substrates, whether carbon or MXene, is an efficient approach to obtain homogenous lithium nucleation during the Li deposition process.

At present, lithiophilic single-atom metals have been proven to be an efficient way to induce lithium nucleation and enhance the electrochemical performance of lithium anodes. However, it

remains unclear whether non-lithiophilic single atoms are useful or what effects they may exhibit. To address this issue, Yan et al. observed that the integration of single-atom Fe into nitrogen-doped carbon (FeSA-N-C) impacted the electron cloud around carbon, creating an effective lithiophilic site that significantly reduced the nucleation overpotential of Li from 18.6 to 0.8 mV. (Figure 7g).[143] Similarly, single-atom Co coordinated to O sites on graphene (Co–O–G SA) as a lithium deposition substrate enables Li overpotential (10.5 mV) decrease than that of graphene (52.4 mV) (Figure 7h).[144] Furthermore, Yang and co-workers fabricate single-atom Co with N, O-coordination materials by the pyrolysis of GO and Co salt.[145] They found that Co—N/O exhibits a lower Li nucleation overpotential (28.8 mV) than those of rGO (51.8 mV) and Co—N (45.2 mV) (Figure 7i). This should be attributed to an enhanced binding ability for Li ions, lower barriers for $Li^+$ to Li° conversion. As a result, the Co—N/O arrangement attains a notable average CE more than 97% at 1 mA $cm^{-2}$ and 2 mAh $cm^{-2}$.[145] These findings highlight the potential of non-lithiophilic single-atom metal-N/O as a promising material for enhancing Li nucleation and battery performance. While non-lithiophilic metals like Fe and Co may not dissolve in lithium, they influence the electron cloud morphology around the single-atom metal, enhancing lithium absorption capability and facilitating nucleation.

Similarly to lithium metal anodes, sodium metal anodes have faced challenges such as uneven metallic deposition, unstable SEI, dendritic growth, as well as substantial volume changes during plating and stripping cycles,[32,146–148] leading to limited reversibility, the occurrence of internal short circuits, safety risks, and shortened cycle life. In response, the single-atom strategy has emerged as a promising solution. By incorporating specific metal single atoms into the anode material, researchers aim to address the aforementioned issues as well as to improve the performance of Na-based energy storage systems.[149,150] Similar to Li-based systems, the use of single-atom materials can potentially enhance the nucleation, deposition kinetics, and stability of Na metal during cycling, leading to improved reversibility and enhanced safety. For example, Yan et al. have devised a method employing carbon-substrate-supported N-anchored Zn atoms as a current collector for Na anodes.[84] These zinc atoms act as strong attractors for $Na^+$, facilitating uniform nucleation of metallic Na and inhibiting dendrite formation (Figure 7j). Consequently, sodium deposition on ZnSA-N-C exhibits a minimal nucleation overpotential of 0 mV (Figure 7k,l), indicating effective removal of nucleation barriers during the sodium plating process. Moreover, these anodes maintain stable voltage response with minimal voltage hysteresis even after 1000 h of cycling, underscoring their long-term stability and practical potential.[84] Similarly, the incorporation of zinc atoms within the carbon shell of ZnSA-HCNT provides abundant sodiophilic (sodium-attracting) sites,[149] effectively lowering the nucleation barrier for sodium plating. Consequently, Na@ZnSA-HCNT anodes demonstrate stable long-term performance in symmetrical battery setups.[149]

### 4.2. Decreasing Local Current Density in 3D Matrix

Single-atom metals have demonstrated strong capabilities in facilitating lithium nucleation during deposition, owing to their high density of active sites. Consequently, combining the single-atom strategy with other proven approaches, such as employing 3D conductive frameworks and SEI, has emerged as a promising route to suppress lithium dendrite growth. Conventional 3D conductive hosts have been widely utilized in lithium-metal anodes to address dendrite formation and improve electrochemical stability.[66,67,151] However, researchers have revealed that Li tends to aggregate predominantly on the host's surface, leaving the interior underutilized. This leads to inefficient use of the available space and a reduction in the energy density of the electrode. To tackle this challenge, researchers have suggested utilizing the high lithiophilic properties of single-atom metals to evenly disperse them within the 3D structure. In contrast to traditional substrate modification strategies, integrating SAMs with a 3D host approach not only facilitates Li nucleation within the structure but also reduces the local current density owing to its porous architecture. For instance, Zhang et al. introduced atomically dispersed $CoN_x$-doped graphene as a host material, facilitating dendrite-free Li deposition (**Figure 8**a,b).[152] Nitrogen doping enables the effective dispersion of Co atoms within the graphene lattice, forming Co—N coordination bonds. The arrangement enhances the local electronic structure, promoting lithium ion adsorption and nucleation (Figure 8c,d). The strong lithiophilicity of the Co—N coordination in the 3D host ensures uniform lithium nucleation and a flat Li plating morphology.[152] These attributes lead to an exceptionally high CE more than 99% at 2 and 5 mA $cm^{-2}$. Moreover, the interconnected 3D structure regulates current density and facilitates efficient mass transfer, resulting in uniform Li deposition with suppressed dendrite formation and mitigated volume expansion.[152] Similarly, an ordered mesoporous N-doped carbon material featuring Ni single atoms (NOMC-Ni) enhances uniform lithium nucleation and growth.[153] The created anode demonstrates a remarkable Coulombic efficiency of 99.8% and sustains a stable voltage hysteresis of 14 mV.[153] Besides, a 3D hierarchical structure of carbon nanosheets anchored with single-atom Co (CC@CN-SACo) demonstrates improved lithophilicity, effectively reducing the nucleation overpotential and showcasing excellent cyclic stability when assembled as a lithium anode.[154]

In prior studies, the strength of interaction between lithium and lithiophilic sites was a key criterion for assessing LMBs. However, Gong et al. challenged this notion, suggesting that lithium-lithiophilic site affinity alone cannot predict LMBs performance.[155] They investigated this by fabricating various SAMs and evaluating their binding energy (Figure 8e). Their findings revealed that a single-atom manganese-doped 3D graphene material (SAMn@NG) exhibits highly reversible lithiophilic sites with optimal adsorption strength for uniform lithium deposition and structural stability (Figure 8f,g).[155] Despite having a higher binding energy than SAZr@NG, SAMn@NG exhibited minimal changes in atomic structures, including bond length and angle around Mn atoms, throughout the lithium plating and stripping processes. This stability translated into significantly improved battery performance for SAMn@NG.[155] These insights provide valuable guidance for designing lithiophilic sites within a 3D conductive host for LMBs, unlocking new avenues for enhancing their performance.

Potassium metal batteries have garnered attention as a compelling alternative to lithium-based systems, owing to

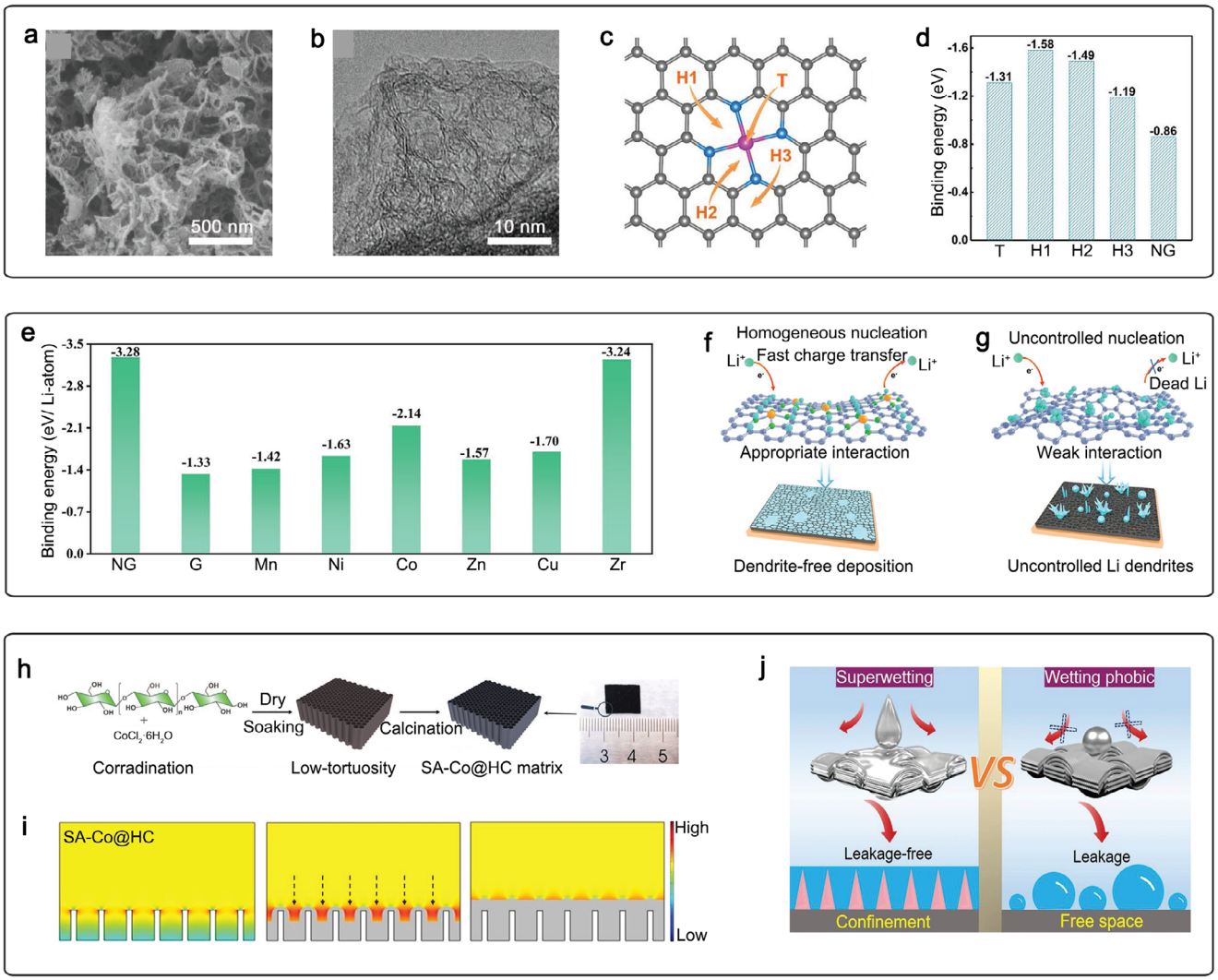


**Figure 8.** a) SEM and b) TEM image of CoNC materials. c) Li adsorption sites on CoNC. d) The summary of binding energies between a Li atom and different adsorption sites on CoNC. Reproduced with permission.[152] Copyright 2018, Wiley-VCH. e) Binding energy of Li atoms on different substrates including graphene, NG, SAMn@NG, SANi@NG, SACo@NG, SAZn@NG, SACo@NG, and SAZr@NG. Schematic illustration of Li deposition on the f) SAM@NG electrode and g) electrode for LMBs. Reproduced with permission.[155] Copyright 2022, Wiley-VCH. h) Schematic of the fabricating process and photograph (right) of SA-Co@HC. i) The morphology evolution and current density distribution snapshots at selected 2D phase-field simulation states during K deposition on SA-Co@HC electrode. Reproduced with permission.[160] Copyright 2023, Wiley-VCH. j) Schematic illustration of liquid NaK Alloy confinement. Reproduced with permission.[161] Copyright 2023, Wiley-VCH.

potassium's natural abundance and low cost. Nevertheless, their practical deployment is hindered by issues such as dendrite formation and the instability of the SEI, which can result in rapid capacity degradation and heightened safety risks.[156–159] Similar to strategies used for Li and Na metals, single-atom strategies hold promise for mitigating potassium dendrite formation and enhancing the performance of potassium-based energy storage systems. Recently, Lu and co-workers developed a composite electrode comprising single Co atoms on 3D N-doped carbon (Figure 8h).[160] Homogeneously supported cobalt on the N-doped carbon enhances potassium deposition kinetics by lowering the nucleation energy barrier as well as uniforming the flux of K ions and electric field (Figure 8i). When tested in a symmetric cell, the SA-Co@HC/K anodes showed remarkable dendrite-free behavior during K deposition and exceptional cycling stability, lasting over 2500 h at 0.5 mA $cm^{-2}$.[160] Furthermore, Co atoms on carbon nanoarrays (Co-SACN) as a superwetting interface on the current collector enhance K adsorption in a NaK alloy (Figure 8j).[161] The resulting Co-SACN@NaK anodes exhibit exceptionally stable plating and stripping processes, with operational lives exceeding 1010 h in $NaClO_4$ electrolyte and 4000 h in $KPF_6$ electrolyte. This electron-rich donor properties of atomic-dispersed Co-SACN enhance electrochemical performance and durability of the anode, marking a significant advancement in efficient K-based energy storage solutions.[161] These progressions present optimistic outlooks for high-efficiency and long-lasting potassium-based batteries. Persistent exploration and innovation in this field will undoubtedly facilitate the practical deployment

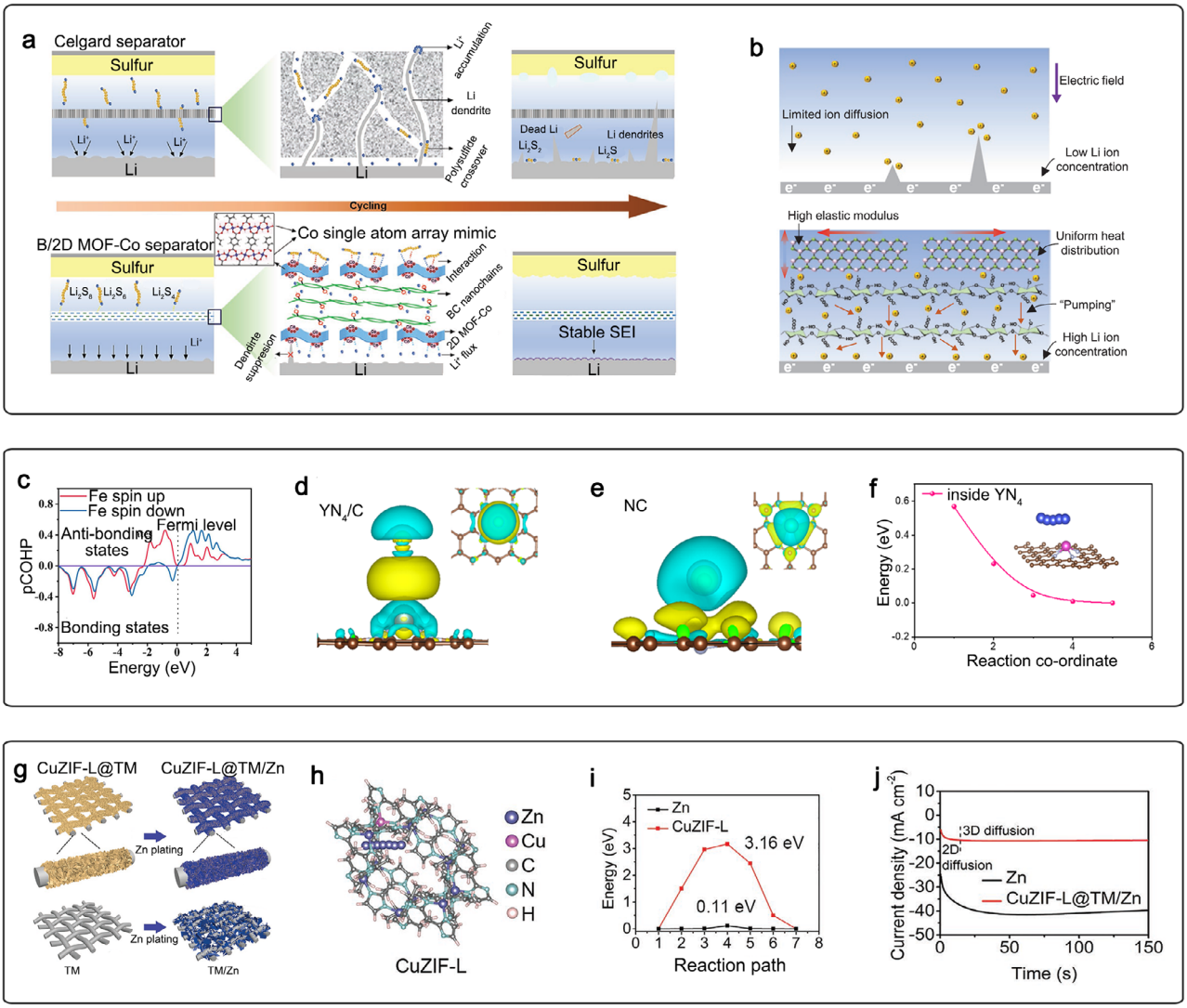


**Figure 9.** a) Schematic illustration for the Li–S batteries with Celgard and B/2D MOF-Co separators. Reproduced with permission.[81] Copyright 2020, Wiley-VCH. b) Schematic illustration demonstrating the effectiveness of BNNs@CNFs based membrane on Li-metal protection. Reproduced with permission.[165] Copyright 2022, Wiley-VCH. c) COHP of Fe—S bond in S@SA Fe-N/S@CNF. Reproduced with permission.[167] Copyright 2023, Wiley-VCH. Top and side views for the charge density difference of Na adsorption on the $YN_4$/C d) and NC e) electrodes; the yellow and blue sections represent the electron accumulation and loss regions, respectively. f) The diffusion energy barrier of Na migration from the graphene lattice to the $YN_4$ moiety. Reproduced with permission.[150] Copyright 2022, by American Chemical Society. g) Schematic illustrations of the Zn depositions on CuZIF-L@TM host and TM host. h) The calculated model of Zn atom diffusion on the surface of CuZIF-L, and i) the related energy profiles on the surfaces of CuZIF-L and Zn. j) Chronoamperograms of CuZIF-L and Zn electrodes in the symmetric cells tested at the overpotential of −150 mV.[169] Copyright 2022, Wiley-VCH.

and widespread adoption of potassium batteries, advancing sustainable and efficient energy storage technologies.

### 4.3. Regulating Metal Ion Flux and Electric Field in SEI

Contrary to substrate nucleation and 3D conductive host strategies, the approach using SAMs combined with protective layers acts as artificial SEI films.[162–164] In this approach, single atoms play a different role in homogenizing $Li^+$ flux and electric field to stabilize the SEI structure. For instance, Guo et al. proposed an ultrathin metal–organic framework (MOF) with a "single atom array mimic" (B/2D MOF-Co), with systematically organized Co atoms coordinated with oxygen atoms ($Co–O_4$ moieties).[81] Subsequently, they integrated single-atom Ru on reduced graphene oxide (rGO@Ru SAs) with a thin functionalized BNNs@CNFs layer.[165] These unique structures enhance the homogeneity of $Li^+$ by promoting strong $Li^+$ adsorption with the single atoms at the interface (**Figure 9**a,b), resulting in a Li symmetrical cell with B/2D MOF-Co exhibiting a low overpotential of only 26 mV and remaining stable for 400 h (Table 5).[165] Meanwhile, a Li//Li symmetric cell with the BNNs@CNFs-based membrane demonstrated a consistent overpotential of 12 mV and sustained stable cycling for 400 h (Table 5).[165] Furthermore, other SAMs serving as protective layers, such as Mo/NG,[166] $Zn_1$-HNC, SACo/ADFS@HPSC, Co-PCNF, and FeCoDACN@PP,

**Table 6.** Electrochemical performance of single-atom materials in Li–S batteries.

| Strategy | Materials | S loading [mg cm$^{-2}$] | Current density [C] | Specific capacity [mAh g$^{-1}$] | Cycles | Ref. |
|---|---|---|---|---|---|---|
| Host | CoSA-N-C | 1.2 | 1 | ≈650 | 1000 | [179] |
| | | 4.9 | 0.2 | ≈880 | 120 | |
| | Co–$N_x$ | 3.5 | 0.2 | ≈460 | 600 | [178] |
| | Co-P cluster/NC | / | 1 | ≈750 | 1000 | [180] |
| | Co-N-C | 4 | 0.75 | 2.2 mAh cm$^{-2}$ | 300 | [29] |
| | $Zn_1$-HNC | 1.5 | 5 | ≈800 | 700 | [181] |
| | SA-Zn-MXene | 1.7 | 1 | ≈700 | 400 | [186] |
| | Co/SA-Zn@NC/CNTs | 2.3 | 1 | ≈650 | 800 | [182] |
| | Mo-N-CNF | 5.1 | 4.27 mA cm$^{-2}$ | ≈600 | 400 | [184] |
| | SATi@CF/s | 4 | 0.5 | ≈800 | 300 | [185] |
| | Ni-NC(p) | / | 0.5 | ≈500 | 600 | [28] |
| | Fe-$N_5$-C | / | 1 | ≈700 | 500 | [167] |
| Separator | FeCoDACN@ PP | 1.56 | 1 | ≈550 | 500 | [194] |
| | Fe/Co-N-HPC | 2.1 | 1 | 694 | 600 | [193] |
| | Pt SAs/$In_2S_3$/$Ti_3C_2$ | 2.1 | 0.5 | ≈800 | 1000 | [187] |
| | Ni@NG | 0.3 | 1 | ≈790 | 500 | [83] |
| | B/2D MOF-Co | / | 0.5 | 700 | 200 | [81] |
| | SA-Co/NGM | 0.156 | 2 | ≈620 | 1000 | [190] |
| | Mn-N-C | 1.2 | 0.2 | ≈500 | 1000 | [188] |
| | FeSA-PCNF | 1.7 | 2 | ≈610 | 500 | [192] |
| | SnSA–NC | 3 | 0.5 | ≈400 | 300 | [195] |
| | Co-NPC | 0.5 | 1 | 601 | 500 | [191] |
| | NC@SA-Co | 1 | 2 | ≈450 | 700 | [242] |
| | Mo/NG | 1 | 1 | ≈680 | 500 | [166] |
| | NiSA-N-PGC | 6 | 0.5 | ≈470 | 600 | [189] |

exhibit exceptional electrochemical performance (Table 5). For example, Mo/NG, comprising molybdenum atoms on graphene, features a unique Mo-$N_2O_2$–C coordination structure.[166] The appropriate binding strength of Mo/NG with $Li^+$ imparts lithiophilic characteristics. Mo/NG redistributes lithium ions at the separator interface, ensuring a uniform lithium-ion flux without hindering $Li^+$ diffusion. The Mo/NG@PP-based cell demonstrates a consistent voltage hysteresis of merely 12 mV after 1000 h (Table 5).[166]

Regarding the combination with a protective layer in Na anodes, atomically dispersed Fe–N/S characterized by a Fe–$N_4S_2$ coordination structure, has been explored for its potential in sodium batteries.[167] The structure enhances the local electronic concentration around the Fermi level (Figure 9c), crucial for promoting uniform Na deposition. The Na@SA Fe–N/S@CNF anode demonstrated excellent voltage polarization and cycling stability in symmetric cells. Besides, Li et al. fabricated the rare-earth metal yttrium (Y) coordinated with four nitrogen atoms (Y–$N_4$) as a promising Janus site for facilitating reversible and uniform Na deposition.[150] The introduction of Y atoms enhances electron density in carbon (Figure 9d,e), thereby significantly reducing the barrier for $Na^+$ transfer (Figure 9f).

Metallic zinc stands out as a prospective anode material for advanced Zn-based batteries owing to its elevated specific capacity and minimal toxicity. Nevertheless, dendrite formation and unwanted reactions at Zn metal anodes pose challenges, affecting both CE and safety, constraining the long-term performance of Zn-based batteries. Moreover, the hydrogen evolution reaction is problematic, particularly in aqueous electrolytes.[45,46,94,168] To address these challenges, Yu et al. have devised a strategy involving atomically dispersed copper within leaf-like Zn-coordinated zeolitic imidazolate framework (ZIF-L@TM).[169] This unique host material incorporates Cu as zincophilic sites, facilitating uniform Zn deposition and preventing dendrite formation during plating and stripping (Figure 9g). Besides, Cu-ZIF-L demonstrates a notably higher Zn migration barrier between adjacent adsorption sites compared to Zn alone (Figure 9h,i), inhibiting 2D atom diffusion of $Zn^{2+}$ on the surface (Figure 9j). Notably, Cu atoms effectively suppress the hydrogen evolution reaction, extending the lifespan of Zn anodes. Consequently, the Cu-ZIF-L@TM/Zn anode demonstrates stable performance, maintaining Zn plating and stripping efficiency for over 1100 h at 1 mA cm$^{-2}$.[169] This innovation holds significant potential for enhancing the durability of Zn-based energy storage systems.

## 5. Li–S and Na–S Batteries

The electrochemical performance of Li–S batteries is intricately tied to both the metal anode and the S cathode. While previous discussions focused on metal anodes, this section delves into the

critical role of S cathodes, crucial for cycle life, rate capabilities, and energy density.[170–173] S cathodes grapple with two primary challenges: the soluble and shuttle effect of polysulfide as well as the slow reaction kinetics between LiPSs and $Li_2S_2/Li_2S$. The shuttle effect of LiPSs presents a substantial challenge due to sluggish conversion between soluble and insoluble intermediates, hindering Li–S battery progress. LiPSs can shuttle to lithium anodes, decreasing S utilization and promoting uneven lithium deposition. Traditional approaches including constructing physical or chemical barriers for LiPSs have limitations, resulting in active material loss and incomplete reactions. To address these challenges, materials capable of LiPSs adsorption have been proposed to prevent their migration. Besides, catalyst materials provide a compelling solution to accelerate reaction kinetics, inhibit the shuttle effect, effectively confine LiPSs, and facilitate the conversion of S species. Among various catalysts, single-atom catalysts (SACs) have garnered considerable interest because of their unique characteristics, including ample catalytic sites, efficient atom utilization, and diminished volume and weight in sulfur cathodes. SACs hold promise in Li–S batteries, serving as both host materials and separators. Beyond Li–S systems, SAMs also show promise in sodium–sulfur (Na–S) batteries. Their integration offers promising prospects for high-energy-density Li–S and Na–S batteries and addresses challenges associated with the shuttle effect of LiPSs or NaPSs migration and reaction kinetics.

### 5.1. SAMs as S Host in Li–S Batteries

The systematic design of sulfur hosts has proven effective in enhancing the performance of Li–S batteries, with optimal hosts exhibiting key characteristics.[174–177] These include excellent electrical conductivity, a structure conducive to containing S/S intermediates and accommodating volume changes, pronounced polar affinity for lithium polysulfides to improve their adsorption, and sturdy catalytic centers for their reversible conversion. Moreover, the integration of catalysts, such as SACs, into sulfur cathodes has been employed to expedite the reversible conversion of lithium polysulfides, addressing challenges related to sluggish reaction kinetics and capacity decline. One promising approach involves integrating single-metal atoms with a 3D S host to construct a multifunctional sulfur cathode, showing great promise for further advancements in Li–S batteries. Various substrates have been utilized for sulfur hosts, incorporating various single-metal atoms (Co, Zn, Fe, Ni, Cu, V, Ru, etc.) in the form of SAMs. For instance, a fibrous framework featuring single-atom $Co—N_x$ dispersion exhibits notable lithiophilic properties and electrocatalytic activity, effectively mitigating the polysulfide shuttle effect and demonstrating impressive performance in integrated Li–S batteries (**Table 6**).[178]

The loading of single atoms typically varies from 0.5 to 2 wt.% in most reported SAMs, which may not maximize their efficiency. Increasing the content of single atoms is thus an effective strategy to enhance the catalytic conversion performance of Li–S batteries. Sun and co-workers have introduced dispersed Co atoms (15.3 wt.%) on N-doped carbon materials (CoSA-N-C) to address multiple challenges in S cathodes.[179] The high content of Co atom catalyst adeptly addresses polysulfide shuttling, accelerates redox kinetics of dissolved polysulfides, and facilitates $Li_2S$ deposition. Dual lithiophilic–sulfiphilic Co-N species in the catalyst critically confine polysulfides and expedite electron and ion transfer. The densely distributed $Co—N_4$ coordinated units function as effective electrocatalytic sites, facilitating conversion between LiPSs and $Li_2S$ (**Figure 10a**). Consequently, CoSA-N-C-based cathodes demonstrate exceptional sulfur utilization, rate performance, and cycle life (Table 6), even under high sulfur loading. Notably, the incorporation of Co atoms enhances $Li_2S_6$ adsorption, reducing volume expansion and achieving excellent cyclic properties at high S loading (Figure 10b,c).[179] In another example, a N-doped carbon matrix supporting a Co–P cluster (Co–P cluster/NC) offers atomic-level dispersion and a high concentration of Co atoms, creating abundant unsaturated Co–P coordination sites. This configuration furnishes dual-atom sites containing both Co and P.[180] These sites play a vital role in dynamically adsorbing/desorbing S species and lithium ions, respectively. The cathode with S@Co-P cluster/NC exhibits exceptional cycling and rate capabilities, achieving a remarkable areal capacity of 6.5 mAh $cm^{-2}$ even with a substantial sulfur loading of 6.2 mg $cm^{-2}$ (Table 6).[180] Similar results have been observed in other single-atom Co-based materials. For instance, a cathode designed with homogenously loaded ZnS nanoparticles and Co—N–C SACs within a highly oriented macroporous host demonstrates impressive performance, eliminating the shuttle effect and corrosion of metallic Li.[29] This cathode delivers high cell-specific energy and maintains Coulombic efficiency over multiple cycles.[29] The improved reactivity of LiPSs resulting from the incorporation of Co atoms contributes to its favorable electrochemical performance (Figure 10d), facilitating the conversion from $S_8$ to $Li_2S$ (Figure 10e).

In addition to single Co atoms, Zn atoms decorated hollow carbon spheres ($Zn_1$-HNC) exhibit excellent properties for Li–S batteries.[181] The nanoreactor's high electronic conductivity, large surface area, and effective active sites facilitate strong physical confinement and chemical anchoring of polysulfide intermediates, leading to exceptional electrocatalysis and prevention of shuttle effects. The fabricated full battery using $Zn_1$-HNC as both the sulfur and lithium electrode demonstrates impressive electrochemical performance, including good cycle stability with low capacity fading, high-rate capability, and high areal capacity with a high S loading (Table 6).[181] Recognizing the individual merits of single Co and Zn atoms, researchers propose integrating them to leverage synergistic effects. A composite catalyst, Co/SA-Zn@NC/CNTs, comprising Co nanoparticles and Zn atoms co-implanted within N-doped porous carbon nanosheets, has been formulated.[182] The active centers of Co and atomic $Zn–N_4$ entities demonstrate optimal charge redistribution, efficiently confining LiPSs and catalyzing their conversion reactions. Li–S batteries utilizing the S cathode based on Co/SA-Zn@NC/CNTs exhibit a remarkable capacity of 1302 mAh $g^{-1}$ at 0.2 C, accompanied by a minimal capacity fading rate of 0.033% per cycle during 800 cycles (Table 6). This dual-atom integrated composite catalyst, exhibiting synergistic effects, holds great potential for enhancing the properties and stability of Li–S batteries.[182] Moreover, another single-metal atom, $Fe—N_5—C$, featuring an oversaturated $Fe–N_5$ coordination structure, has been proposed by Chen and colleagues.[183] This catalyst demonstrates the ability to adsorb polysulfides through chemical interaction and enhance the redox reaction kinetics, effectively reducing the shuttle effect.

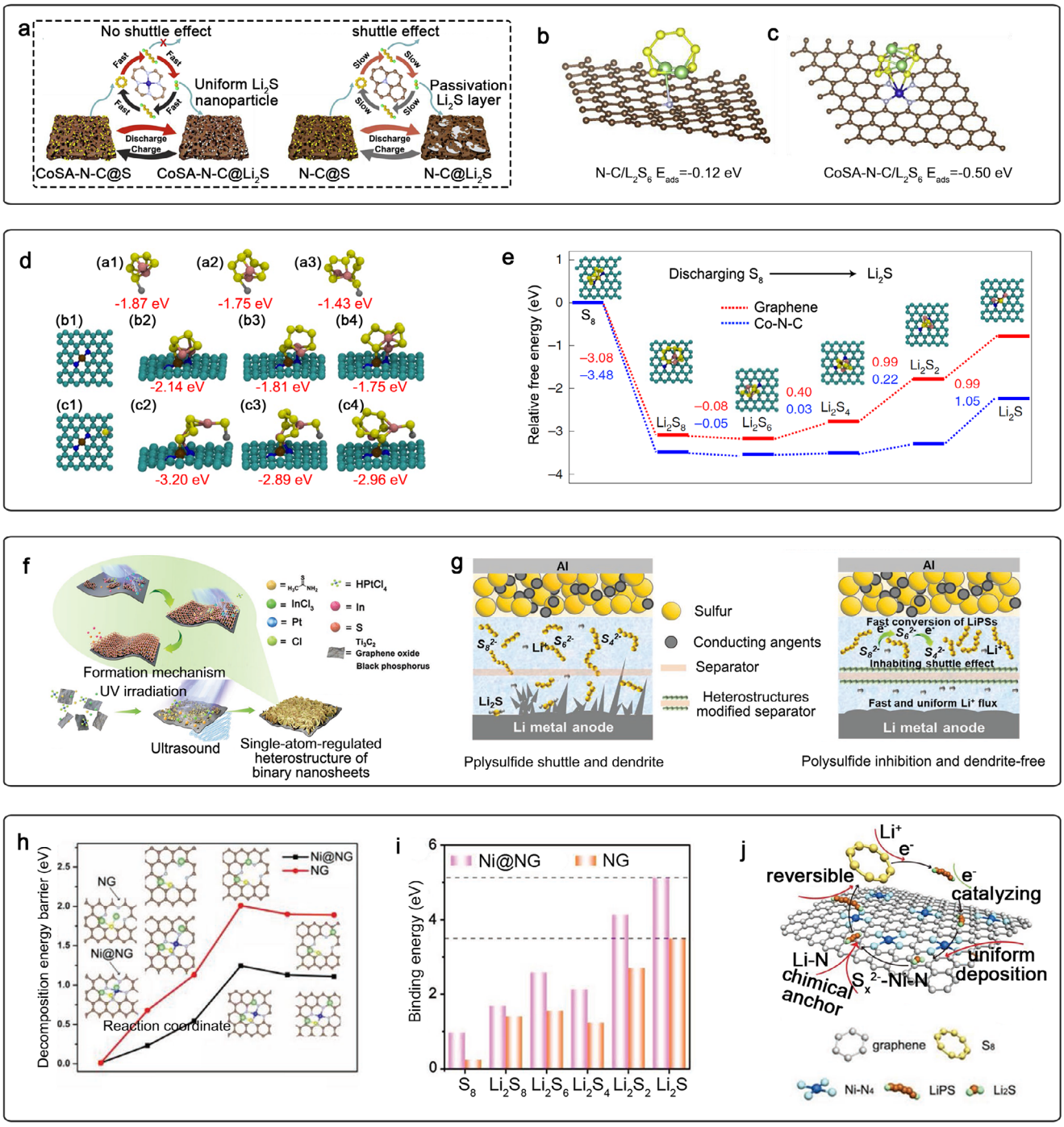


**Figure 10.** a) Schematic illustration of the effect of CoSA-N-C in improving the conversion kinetics between the solid (S, $Li_2S$) and liquid (polysulfides), and mediating the deposition of lithium sulfide nanoparticles. b) and c) Atomic conformations and binding energy for $Li_2S_6$ species adsorption on N-C and CoSA-N-C based on DFT calculations. Here, the brown, yellow, green, white, and blue balls represent C, S, Li, N, and Co atoms, respectively. Reproduced with permission.[179] Copyright 2020, Elsevier Ltd. Density functional theory calculations. d) Optimized configurations of $Li_2S_4$, $Li_2S_6$ and $Li_2S_8$ absorption on ZnS (a1–a3), the Co—N—C surface (b1–b4) and the ZnS, Co—N—C surface (c1-c4). The yellow, pink, silver, brown, blue, and cyan balls denote the S, Li, Zn, Co, N, and C atoms, respectively. e) Relative free energy for the discharging process from $S_8$ to $Li_2S$ on the bare graphene and Co—N—C surfaces. The optimized structures of the intermediates on the Co—N—C surface are shown as the insets. Same color coding for atomic structure as in d). Reproduced with permission.[29] Copyright 2020, Nature Publishing Group. f) Schematic representation for the fabrication of SA-regulated heterostructure of binary nanosheets through an ultrasound-assisted photochemical reduction strategy. g) Schematic illustrations of polysulfides suppressing and Li anode deposition process on PP and heterostructures modified PP separator. Reproduced with permission.[187] Copyright 2022, Wiley-VCH. h) The decomposition energy barriers of $Li_2S$ on the Ni@NG or NG. i) Binding energies between the LiPS and the Ni@NG or NG. j) The catalytic mechanism of the LiPS on the surface of Ni@NG in the electrochemical process. Reproduced with permission.[83] Copyright 2019, Wiley-VCH.

Full cells utilizing a composite cathode of S/Fe-$N_5$-C exhibit excellent rate capability and high areal capacities, even under elevated S loading conditions (Table 6).[183] However, the cyclic stability of Li–S should be further improved. In pursuit of enhanced redox kinetics, Ni-NC(p), a mesoporous nanostructure decorated with single-Ni atoms, characterized by thin outer shells and porous inner networks, has been developed.[28] The single-Ni atoms act as catalysts, enhancing the redox kinetics of LiPSs. When combined with S, the Ni-NC(p)/S composite exhibits a high discharge capacity of over 960 mAh $g^{-1}$ (Table 6).[28] Furthermore, Mo–$N_4$ atoms incorporated into an N-doped carbon structure (Mo-N-CNF) serve as a cathode material for S hosts.[184] The single Mo–$N_4$ atoms regulate the hydrophilic property, $Li^+$ diffusion, and catalytic conversion of LiPSs within the Mo-N-CNF structure, demonstrating a good specific capacity of 1248 mAh $g^{-1}$ at 0.2 C (Table 6).[184] These results highlight the potential of Mo-N-CNF as an S host cathode for Li–S batteries.

It's notable that while transition metal elements like Fe, Co, and Ni are well-established for their excellent catalytic activity in Li–S batteries, Ti, despite being a transition metal element, has received less attention. In a recent study, Chen et al. proposed that the catalytic activity of single-atom Ti catalysts in Li–S batteries is regulated by the hybridization of *d-p* orbitals between metallic Ti atoms and sulfur species.[185] Transition metals with lower atomic number, such as Ti, manifest fewer occupied anti-bonding states, facilitating LiPSs binding and catalyzing their electrochemical reactions. Utilizing a controllable nitrogen coordination approach, 3D electrodes incorporating SACs (Mn, Cu, Cr, and Ti) were investigated. Notably, Ti atoms embedded in electrodes exhibited the least electrochemical barrier for LiPSs reduction/$Li_2S$ oxidation and the highest catalytic activity. The highly active catalytic site of Ti atoms on the conductive transport network facilitated elevated S utilization with low catalyst loading (1 wt.%) and high S loading (8 mg $cm^{-2}$) (Table 6).[185] Another crucial factor affecting Li–S battery performance is the low electrical conductivity of the S cathode, leading to significant voltage polarization and poor cycle life. Addressing this issue, Yang et al. proposed utilizing atomic Zn on MXene layers as an efficient catalyst. The high conductivity of 2D MXene reduces energy barriers for polysulfide conversion and forms strong interactions with polysulfides due to its high electronegativity. Besides, homogeneously dispersed Zn atoms promote the initiation of $Li_2S_2$/$Li_2S$ formation on MXene layers during redox processes.[186] Consequently, the S cathode incorporating MXene with single-atom Zn implantation demonstrates notable characteristics, including a substantial capacity (1136 mAh $g^{-1}$), impressive areal capacity (5.3 mAh $cm^{-2}$), excellent rate capability (640 mAh $g^{-1}$ at 6 C), and robust cycle stability following electrode optimization (Table 6).[186]

### 5.2. SAMs-Based Separator in Li–S Batteries

The 3D S host strategy offers promising electrochemical performance in Li–S batteries, but its porous structure significantly reduces the energy density. To address this, constructing a separator has emerged as an effective approach for suppressing the shuttle effect and accelerating reaction kinetics without compromising energy density. For instance, a heterostructure of Pt atoms immobilized $In_2S_3/T_{i3}C_2$ nanomaterial (Pt-SAs/$In_2S_3/T_{i3}C_2$) has been developed as the separator (Figure 10f).[187] This heterostructure effectively suppresses polysulfide migration and exhibits good electrocatalytic activity for LiPSs decomposition (Figure 10g). Cells with modified separators demonstrate a high initial discharge capacity of 1068.4 mAh $g^{-1}$ at 0.5 C and excellent rate property (Table 6).[187] While Pt single atoms offer efficient catalytic properties, their high cost increases the overall price of Li–S batteries. Therefore, alternative non-noble metals such as Mn, Ni, Co, and Fe are considered. For instance, atomically dispersed manganese-nitrogen-doped porous carbon (Mn—N—C) material adsorbs polysulfides and enhances electrical conductivity.[188] When used to modify a separator, Mn—N—C exhibits exceptional conductivity, robust immobilization, and outstanding catalytic performance, facilitating polysulfides conversion and $Li_2S$ nucleation/dissolution. The Li–S cell with this modified separator achieves an impressive initial discharge capacity of 1596 mAh $g^{-1}$ at 0.1 C (Table 6).[188] Besides, single Ni atoms integrated into N-doped graphene (Ni@NG) featuring a Ni–$N_4$ coordination are employed for the modification of separators in Li–S batteries.[83] The Ni–$N_4$ coordination effectively traps polysulfides, forming strong Ni—N bonds and facilitating electron transfer. The interaction between LiPSs and oxidized Ni sites results in reduced free energy and a low energy barrier for LiPSs conversion (Figure 10h–j). Besides, within a N-doped graphitic carbon substrate, the Ni–$N_4$ coordination enhances the transfer kinetics and immobilizes them effectively to curb the shuttle effect.[189] Consequently, Li–S battery with separators modified by Ni@NG[83] or NiSA-N-PGC[189] exhibit robust and sustained cycling stability (Table 6).

While Ni–$N_4$ demonstrates good cycle performance, enhancing rate capability remains crucial. In contrast, Co—$N_4$ coordination consistently exhibits excellent rate performance at high current densities. For instance, Co atoms implanted into a carbon matrix enhance $Li^+$ reaction kinetics, facilitating fast conversion rates in ultrahigh-rate. The introduction of Co atoms reduces the $Li^+$ diffusion barrier on the carbon surface, resulting in improved performance at high rates. The $Li_2S$ electrode, derived from cost-effective $Li_2SO_4$ precursors, demonstrates a notable rate capacity (441 mA h $g^{-1}$ at 10 C) and an extended lifespan of 1500 cycles at 2 C (Table 6). Similarly, the single Co atoms on nitrogen-doped graphene mesh (SA-Co/NGM) catalyst promote efficient catalytic conversion of LiPSs in the S cathode.[190] This planar Co—$N_4$ coupling within the N-doped graphene mesh maximizes Co atom utilization, facilitating efficient conversion of LiPSs. Enhanced exposure of Co—$N_4$ sites regulates sulfur electrochemistry, effectively suppressing the shuttle effect and accelerating bidirectional sulfur reaction kinetics through electron delocalization. When employed as a separator in full cells, this SA-Co/NGM demonstrates outstanding performance, achieving a high rate performance of 649 mAh $g^{-1}$ at 5 C (Table 6).[190] However, achieving excellent rate capabilities alone is not sufficient; high areal capacity is also crucial. High areal capacity implies a thick sulfur cathode, high sulfur loading, and ultimately, high energy density. Given the substantial volume fluctuation of the sulfur cathode throughout repetitive discharge–charge cycles, achieving a high areal capacity poses a notable challenge. To address this, a Co-NPC nanomaterial, featuring homogeneous dispersion of Co atoms within a N-doped porous carbon nanosphere, is developed.[191] The numerous active centers in Co-NPC actively participate in S

redox reactions, leading to efficient and rapid polysulfide conversions. Li–S batteries incorporating the Co-NPC separator exhibit markedly improved specific capacity and long-term cycle life, achieving an exceptionally high areal capacity of 7.92 mAh $cm^{-2}$ when the S loading is increased to 6.2 mg $cm^{-2}$ (Table 6).[191]

In addition to Co atoms, Fe atoms also exhibit excellent rate capabilities and high areal capacity performance. For instance, Fe single atom decorated porous carbon nanofibers (FeSA-PCNF) facilitate rapid charge transfer and provide plentiful active interfaces for LiPS conversions.[192] The highly active $FeN_4$ sites exhibit strong chemisorption and efficient electrocatalytic conversion for LiPSs. Full cells composed of FeSA-PCNF show outstanding electrochemical properties, including a high rate capability of 791 mA h $g^{-1}$ at 5 C (Table 6).[192] Furthermore, Fe/Co-N-HPC is an efficient catalyst comprising N-coordinated binary metal atoms embedded in a porous carbon matrix.[193] This catalyst effectively traps and catalyzes the conversion of polysulfides in the S cathode. The incorporation of Co atoms enriches the electron density of the Fe sites, leading to a synergistic catalytic effect and improved catalytic performance of the S cathode. Full cells equipped with the resulting separator demonstrate exceptional rate properties and excellent long cycle life. Moreover, by improving the S loading up to 4.8 mg $cm^{-2}$, an impressive areal capacity of 6.13 mAh $cm^{-2}$ is obtained (Table 6).[193] Considering the crucial roles played by both Co and Fe atoms in high-rate and high areal capacity lithium–sulfur batteries, combining the two could potentially lead to even better performance. Thus, a modified separator is constructed by doping Fe and Co atoms into a 3D ZIF-8 matrix (FeCoDACN@PP).[194] This modified separator exhibits a synergistic catalytic effect that effectively inhibits the shuttle effect of LiPSs on the S cathode. The FeCoDACN@PP separator, composed of Co and Fe atoms, shows promising properties in Li–S batteries, delivering a high specific reversible capacity of 1404 mAh $g^{-1}$ at 0.1 C.[194] The FeCoDACN@PP modified separator demonstrates its potential to promote the properties and cycling stability of LSBs.

Transition metal SAMs have been widely investigated for catalytic conversion in Li–S batteries. However, exploring the catalytic potential of non-transition metals, such as main group elements, is an area of interest. In this regard, a single-atom Sn-based catalyst (SnSA-NC) featuring $Sn–N_4$ sites has been developed.[195] The strong interaction between Sn and N atoms creates a highly polar site that effectively adsorbs polysulfides. Particularly, the p band of the Sn atoms adjusts the energy barriers for crucial steps in S redox, facilitating the conversion of LiPSs. By incorporating SnSA-NC into the separator, S utilization increases to 79.7%, leading to significantly improved cyclability and rate performance in Li–S cells (Table 6).[195] This catalytic enhancement highlights the potential of SnSA-NC in enhancing the efficiency and stability of Li–S batteries.

### 5.3. SAMs in Na–S Batteries

Na–S batteries are increasingly recognized as a promising next-generation technology for large-scale energy storage due to their high theoretical energy density (1672 mAh $g^{-1}$), abundance of raw materials, and low cost.[196–199] In particular, room-temperature Na–S batteries offer the potential for safer and more accessible operation compared to their high-temperature counterparts. However, their practical application is severely hindered by several key challenges.[200–204] Similar to Li–S batteries, these include the severe shuttle effect of sodium polysulfides (NaPSs), which causes active material loss and rapid capacity decay; the poor conductivity of sulfur and its discharge products, which leads to sluggish reaction kinetics; the typically low sulfur loading (<65 wt.%), which limits the practical energy density; and the irreversible deposition of $Na_2S$, which compromises cycling stability. In recent years, SACs have emerged as a powerful strategy to address these issues due to their high atomic efficiency, unique electronic properties, and highly tunable coordination environments.[205–215]

To solve these issues, Chen and his co-workers introduce an orbital engineering strategy by optimizing the s-p orbital overlap between sodium polysulfides and single-atom indium catalysts.[214] Traditional p-block metal catalysts lack d-electrons and are often limited in catalytic activity. To overcome this, the researchers designed indium SACs with tailored nitrogen coordination environments, such as NG-$InN_5$, which maximize the s-p orbital overlap degree between the Na atoms in NaPSs and the p-orbitals of In. The NG-$InN_5$ structure showed the highest value (0.055), significantly enhancing electron transfer and lowering the energy barriers for both the sulfur reduction and oxidation reactions (as low as 0.86 eV). As a result, the assembled pouch cell demonstrated excellent cycling performance, retaining 490.7 mAh $g^{-1}$ after 70 cycles at 2 A $g^{-1}$, with a high coulombic efficiency of 96% (**Table 7**). This work establishes a direct relationship between orbital overlap and catalytic activity, offering valuable insights for the rational design of p-block metal SACs.[214] Besides, Dou et al. address the issue of sluggish ion/electron transport in conventional SACs by constructing linearly interlinked Fe-$N_x$-Fe single-atom chains (IFeSACs) embedded in a graphitized carbon framework.[209] The linear chains provide a delocalized electron network, significantly enhancing the conversion kinetics of sulfur species. Meanwhile, the carbon scaffold is engineered with pillar-like channels and an optimized interlayer spacing of 0.347 nm to facilitate fast $Na^+$ diffusion. This synergistic structure enables exceptional rate performance: the RT Na–S cell delivers 325 mAh $g^{-1}$ even after 5000 cycles at a high current density of 10 A $g^{-1}$, with a minimal capacity decay of only 0.013% per cycle (Table 7). This work presents a novel approach to integrate atomically dispersed active sites with ion transport pathways, effectively bridging the gap between catalytic activity and rate capability.[209] Furthermore, researchers addressed the trade-off between high sulfur loading and electrochemical reversibility by constructing a cathode with atomically dispersed dual-active sites based on $MoS_2$-$Mo_1$ clusters anchored on a sulfur-doped graphene framework.[205] This hybrid catalyst forms a delocalized electronic system that not only stabilizes NaPSs but also accelerates their conversion. Remarkably, the cathode achieves an ultra-high sulfur content of 80.9 wt.%, one of the highest reported values for Na–S batteries. The cell delivers an initial capacity of 1017 mAh $g^{-1}$ and maintains 505 mAh $g^{-1}$ after 1000 cycles, corresponding to a low decay rate of 0.05% per cycle (Table 7).[205] DFT calculations reveal that the $Mo_1$ sites, with a d-band center of −0.41 eV, provide strong $Na_2S$ adsorption energy (−14.66 eV), thereby facilitating the conversion of intermediate polysulfides. This dual-site strategy effectively resolves the long-standing

**Table 7.** Electrochemical performance of single-atom materials in Na–S batteries.

| Materials | S loading | Current density | Specific capacity [mAh $g^{-1}$] | Cycles | Ref. |
|---|---|---|---|---|---|
| Fe1@NC@S | 68% wt.% | 0.3 A $g^{-1}$ | ≈430 | 1300 | [196] |
| Cu SA/NOC/S-2 | 67% wt.% (2–2.5 mg $cm^{-2}$) | 1 A $g^{-1}$ | ≈580 | 1000 | [198] |
| 3D-PNCV@S | 44.39 wt.% | 5 A $g^{-1}$ | ≈450 | 800 | [203] |
| S@$MoS_2$-Mo1/SGF | 0.96 mg $cm^{-2}$ | 0.1 A $g^{-1}$ | ≈500 | 1000 | [205] |
| Zn-$N_2$/CF/S | / | 10 A $g^{-1}$ | ≈400 | 4000 | [212] |
| S@SA Fe-N/S@CNF | 4 mg $cm^{-2}$ | 1 A $g^{-1}$ | ≈600 | 500 | [201] |
| S@Fe/NC/700 | 4–4.5 mg $cm^{-2}$ | 10 A $g^{-1}$ | ≈310 | 5000 | [209] |
| S/NHC-$InN_5$ SAC | 1.5 mg $cm^{-2}$ | 1 A $g^{-1}$ | 384.9 | 800 | [214] |
| S@Mn1-PNC | 2.6 mg $cm^{-2}$ | 2 A $g^{-1}$ | 344.1 | 3000 | [207] |
| Ca-$O_4$N-C@S | 1 mg $cm^{-2}$ | 3 C | 887.1 | 800 | [215] |
| $MoS_2$/MoSAC/CF@S | 47.3 wt.% | 1 A $g^{-1}$ | 441.38 | 400 | [213] |
| Zn–$N_2$@NG/S | 66% | 2 A $g^{-1}$ | 293 | 6500 | [202] |
| Y SAs/NC-S | 1.4 mg $cm^{-2}$ | 5 A $g^{-1}$ | 510 | 1000 | [200] |
| $Co_1$–ZnS/C@S | 5 mg $cm^{-2}$ | 0.1 A $g^{-1}$ | 640 | 500 | [197] |

conflict between sulfur content and cycle stability, pushing Na–S batteries closer to practical application.[205]

These studies demonstrate the vast potential of SACs in enhancing the electrochemical performance of NasS batteries. By engineering the electronic structure through orbital overlap optimization, innovating structural frameworks such as linear atom chains and ion transport channels, and introducing atomically dispersed dual-active sites, researchers have significantly advanced the catalytic efficiency, sulfur utilization, and cycle life of these systems.

## 6. Metal–Air Batteries

Similar to Li–S batteries, metal–air batteries (Li–$O_2$, Na–$O_2$, and Zn–air) have attracted considerable scientific interest owing to their exceptionally high theoretical energy density.[216,217] For instance, Li–$O_2$ batteries possess ≈3500 Wh $kg^{-1}$, nine times greater than that of contemporary LIBs (≈400 Wh $kg^{-1}$), making them significantly appealing for long-range electric vehicle applications. However, efficient catalysis of ORR and OER at the cathode presents challenges, directly impacting the batteries' electrochemical properties. Therefore, the development of an efficiently catalyzed cathode is imperative. Single-atom catalysis, with its high utilization of metal atoms, has demonstrated exceptional catalytic properties, leading to good cyclic stability and rate capabilities in metal–air batteries.

In Li–$O_2$ batteries, the cathode drives the ORR during discharge, forming $Li_2O$ and $Li_2O_2$. However, the final product $Li_2O_2$ possesses low electrical conductivity, resulting in a significant increase in local electrical resistance and overpotential, limiting rate capacity and cyclic life. During charge, OER decomposes $Li_2O_2$ into $Li^+$ and $O_2$, with slow kinetics due to $Li_2O_2$ presence, limiting the high-energy-density properties. Noble metals such as Ru, Pt, and Pd excel in ORR and OER catalysis, prompting their single-atom application in Li–$O_2$ batteries. For instance, Xu et al. fabricated an electrocatalytic material incorporating single-atom Ru on N-doped porous carbon (Ru SAs-NC) (**Figure 11a**).[30] The $Ru_{0.3}$-SAs-NC catalyst in Li–$O_2$ cathode significantly reduces the overpotential (≈0.55 V), attributed to the crucial role of Ru–$N_4$ configuration as a driving force center. Moreover, the abundant Ru—$N_4$ substantially influences the inherent interaction with intermediate species in the electrochemical reactions.[30] This is credited to the inclusion of Ru atoms, which significantly reduces the free energy of reactions (Figure 11b). The charge density difference indicates an enrichment of charge, providing supporting evidence (Figure 11c). Similarly, Lei et al. engineered a monoatomic Pt catalyst anchored on porous ultrathin g-$C_3N_4$ nanosheets (Pt-CNHS), showcasing high dispersibility and stability.[218] This design results in improved utilization efficiency and enhanced electrochemical activity. Besides, employing atomically dispersed Pd loaded on N-doped carbon spheres as cathode catalysts has demonstrated notable advantages.[219] The Pd-$N_4$ coordination enables the regulation of $Li_2O_2$ product morphology and distribution, optimizing decomposition reversibility. The unique configuration of Pd–$N_4$ facilitates electron transfer between Pd and neighboring N atoms, inducing a positive charge on Pd and a downshift in the d-band center.[219] As a result, Li–$O_2$ batteries employing Pd-SAs/NC cathodes demonstrate minimal charge overpotential of 0.24 V and sustained cycling stability with low overpotentials at 500 mA $g^{-1}$.[219]

Furthermore, transitioning to non-noble single-atom catalysis presents a promising avenue to reduce the cost of Li–$O_2$ batteries, advancing their practical application. To this end, Liu et al. investigated a series of non-noble single-atom catalysts, each supported on an array of $Co_3O_4$ nanosheets grown on carbon cloth.[220] Notably, among these catalysts, Ni-SA-$Co_3O_4$/CC exhibited the highest catalysis performance for ORR and OER conversions. The catalytic activity of the diverse metal atoms in the catalysts primarily hinges on the reaction barrier on the active centers and the interaction between the incorporated metal atoms and the key reactants.[220]

Similar to Li–$O_2$ batteries, in Na-$O_2$ batteries, the generation and decomposition of $Na_2O_2$ on the cathode during the discharge/charge cycle are predominant processes. While noble

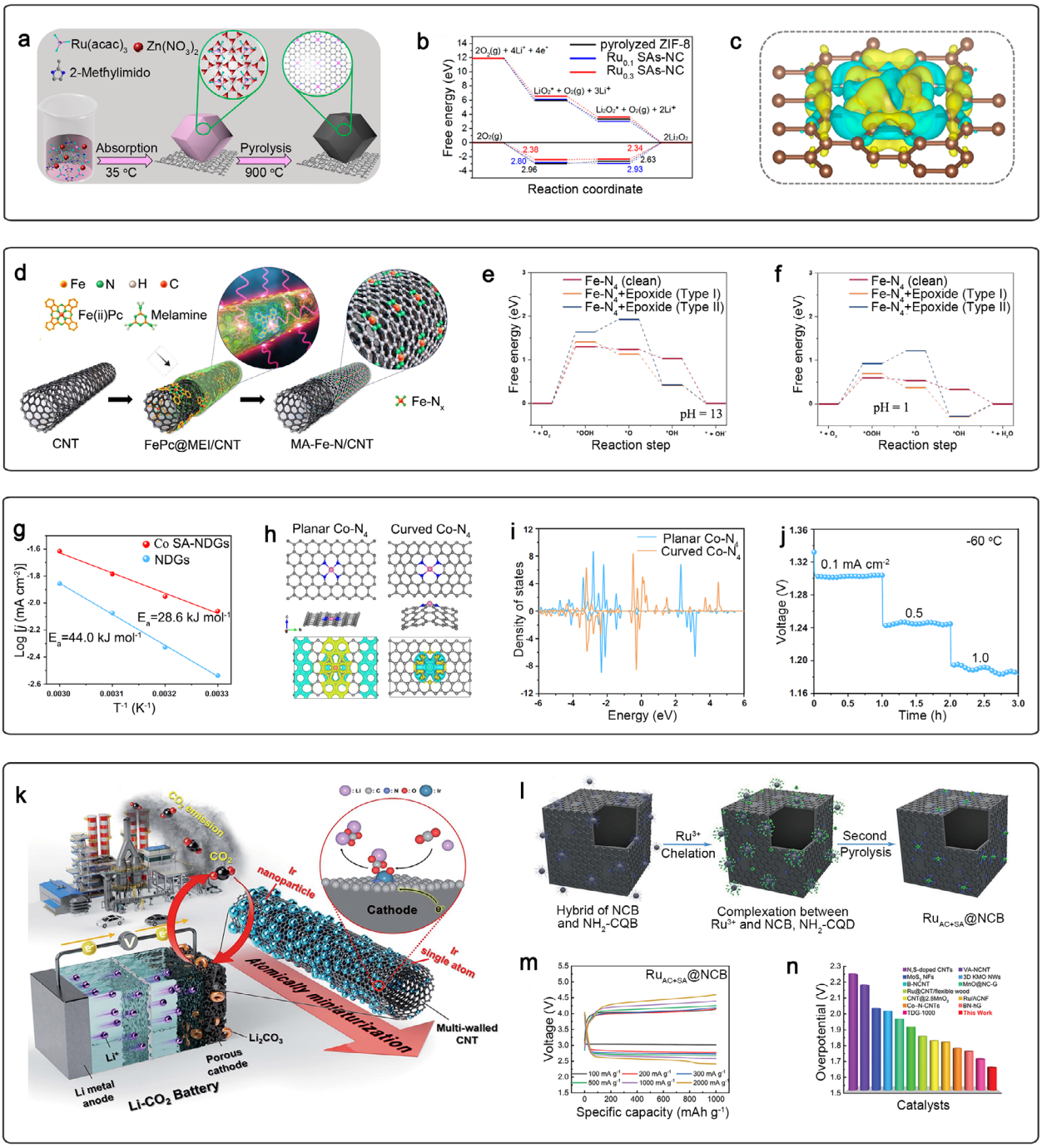


**Figure 11.** a) Scheme of the formation of Ru SAs-NC on the flexible CC. b) Gibbs free energy diagrams at 2.97 V for the discharge/charge reactions on the active surface of pyrolyzed ZIF-8, $Ru_{0.1}$SAs-NC, and $Ru_{0.3}$SAs-NC. c) Corresponding charge density distribution of $Ru_{0.3}$SAs-NC. Isosurface level = 0.002 au. Reproduced with permission.[30] Copyright 2020, by American Chemical Society. d) Schematic preparation of the MA-Fe-N/CNT catalyst via selective microwave annealing. e) and f) Calculated free-energy evolution diagram for the ORR on the central Fe site under the same electrode potential of $U = 1.23$ versus RHE with pH of 13 and 1, respectively. Reproduced with permission.[221] Copyright 2020, by Royal Society of Chemistry. g) Arrhenius plots of Co SA-NDGs and NDGs at the overpotential of 350 mV. h) Established models of planar Co—$N_4$ site and curved Co—$N_4$ site. Calculated differential charge density. Yellow and cyan areas represent charge density aggregation and depletion, respectively. i) Density of states for planar Co—$N_4$ site and curved Co—$N_4$ site. j) Rate performance of the CoSA-NDGs-based quasi-solid-state ZABs at −60 °C. Reproduced with permission.[225] Copyright 2022, Nature Publishing Group. k) Schematic illustration of the Li–$CO_2$ battery employing atomically minimized $IrO_x$/Ir bi-phase catalysts and the mechanism through which they catalyze the Li–$CO_2$ reaction. Reproduced with permission.[236] Copyright 2022, by Royal Society of Chemistry. l) Schematic illustrating the synthesis procedure for RuAC+SA@NCB. m) Discharge/charge curves of RuAC+SA@NCB cell tested at current densities from 100 to 2000 mA $g^{-1}$. n) Comparison of overpotentials at 1 A $g^{-1}$ for RuAC+SA@NCB with the state-of-the-art catalysts in the literature. Reproduced with permission.[237] Copyright 2022, Wiley-VCH.

metal catalysis exhibits good catalytic activity, its durability over long-term cycles is a concern. Therefore, durability and cycle life are crucial for catalysts. Non-noble single-atom catalysis has thus been extensively explored in Na–$O_2$ batteries. For instance, the Fe-$N_4$/CNT catalyst, featuring N-coordinated Fe atoms on carbon nanotubes, exhibits remarkable ORR performance and universal durability across various pH values (Figure 11d), outperforming expensive Pt/C catalysts.[221] The plentiful Fe–$N_4$ centers in the catalyst contribute to its exceptional performance, with a half-wave potential of 0.92 V.[221] DFT studies further demonstrate that clean sheets exhibit more favorable *OOH adsorption than Type I and Type II, suggesting that O functional groups like epoxides on carbon structures hinder the 4-electron ORR pathway on the Fe–$N_4$ site, especially in acidic conditions (Figure 11e,f). Moreover, Huang et al. have investigated the catalytic behavior of single-atom Co/reduced graphene oxide (SA-Co/rGO) in Na–$O_2$ nanobatteries using real-time imaging in an environmental TEM.[222] The investigation reveals that $Na_2O_2$ spheres form on the SA-Co/rGO scaffold during discharging, facilitating decomposition during charging. This contrasts with the sluggish process observed on bare rGO without single-atom catalysts. A coin cell Na–$O_2$ battery with an SA-Co/rGO air cathode outperforms a bare rGO cathode. DFT calculations underscore the crucial role of the local coordination environment (Co—$N_4$) in fine-tuning charge density and oxidation states, activating $O_2$ molecules, and facilitating the ORR/OER processes.[222] This highlights the potential of SA-Co/rGO as a catalyst to enhance Na–$O_2$ battery performance.

Metal-air batteries like Li–$O_2$ and Na–$O_2$ batteries, known for their high energy density, face challenges due to the requirement of a pure oxygen environment and sensitivity to humidity. In contrast, Zn–air batteries operate in an aqueous electrolyte, using $OH^-$ as the reaction medium. During discharge, the Zn anode reacts with $OH^-$ to form $Zn(OH)_4$. The consumed $OH^-$ is replenished by the reduction of $O_2$ at the cathode. The charging process involves the reverse of this reaction. SAMs are crucial in Zn–air batteries. Qian et al. proposed single-atom-dispersed Co—N—C and Fe—N—C cathodes to accelerate ORR and OER kinetics, enabling a Zn–air battery with enhanced stability.[223,224] The Co—N—C nanomaterial exhibits a high half-wave potential (0.89 V) and a comprehensive oxygen electrode potential gap of 0.72 V.[224] The incorporation of Co/Fe atoms in catalysts enhances reactivity and facilitates the chemisorption of oxygen intermediates during battery operation, promoting improved performance.[223] Consequently, the rechargeable Zn–air battery exhibits excellent reversibility and stability, maintaining a negligible voltage gap change of 0.04 V over 1000 cycles.[223] Besides, Xiong et al. fabricated single-atom Co anchored on graphene (CoSA-NDGs) for solid-state Zn–air batteries.[225] The CoSA-NDGs catalyst lowers cathode reaction activation energy (Figure 11g), elevates localized charge densities (Figure 11h), and facilitates oxygenated intermediates adsorption (Figure 11i), ensuring good electrochemical performance even at low temperatures (Figure 11j).[225] Furthermore, the NMCS-rGO-Co catalyst, with single Co atoms within a dual-carbon architecture featuring a sandwich-like porous N-doped structure, exhibits outstanding performance.[226] It utilizes plentiful Co—$N_4$ centers and a well-designed porous structure to create stable three-phase reaction interfaces, allowing for fast electron transfer, increased oxygen and electrolyte diffusion, and efficient water removal. When applied in neutral Zn–air batteries, the NMCS-rGO-Co catalyst exhibits robust stability, enabling continuous discharge for 36 h under 50 mA $cm^{-2}$.[226]

Despite the presence of Co atoms, Fe atoms also exert a significant effect in Zn–air batteries. For instance, the Fe-N-C-KCl catalyst exhibits a high half-wave potential of 0.877 V and a maximum power density of 185 mW $cm^{-2}$ for Zn–air battery, surpassing Pt/C catalysts.[227] Li et al. developed a CNT-supported Fe—N—C nanomaterial with a half-wave potential of 0.865 V for ORR.[228] The incorporation of CNTs significantly reduces the overpotential by 310 mV compared to Fe—N—C alone. This catalyst enables Zn–air batteries with a peak power density up to 182 mW $cm^{-2}$ and exceptional cycle life, outperforming commercial Pt-C catalysts and the majority of previously reported catalysts.[228] Additionally, 3D N, S co-doped carbon nanomaterials with densely distributed Fe single-atom nanoclusters (Fe-SA-NCs) are synthesized by modulating the Fe-to-TA (thiourea) molar ratios.[229] These catalysts outperform Pt/C catalysts, exhibiting higher half-wave potential, onset potential, kinetic-limited current density, and better long-term stability.[229] When used as air electrodes in Zn–air batteries, they offer higher specific capacity than conventional Pt/C catalysts, showcasing the efficiency of Fe—N—C for the ORR in Zn–air batteries. Notably, the utilization of purified waste pig blood as a carbon source enables the synthesis of 2D sheet-like porous single-atom catalysts.[230] These catalysts contain single Fe sites originating from hemoglobin, exhibiting excellent ORR activity. Mesopores formed through Zn activation during $NH_3$ pyrolysis facilitate efficient mass transfer.[230] Specifically, the Zn-incorporated Fe catalyst demonstrates promising performance in the conversion of ORR and OER, achieving maximum power densities of 352 mW $cm^{-2}$, highlighting its potential for high-power applications.[230] Moreover, He et al. have introduced a dual-metal-site bifunctional catalyst featuring atomically dispersed $FeN_4$ and $NiN_4$ in N-doped graphene (Fe/Ni(1:3)-NG).[231] This combination enhances catalytic performance, with the Fe/Ni(1:3)-NG catalyst demonstrating highly effective bifunctional catalytic activity and a half-wave potential of 0.842 V for the ORR.[231] Utilizing these bifunctional catalytic activities, a zinc–air battery composed of Fe/Ni(1:3)-NG demonstrates a good power density of 164.1 mW $cm^{-2}$.[231] These catalysts exhibit significant potential for utilization in energy storage systems, particularly in the context of Zn–air batteries.

Li–$CO_2$ batteries, emerged around 2013, have seen significant advancements in understanding their reaction mechanism and addressing associated challenges. During discharge, a $CO_2$RR occurs at the cathode, forming $Li_2CO_3$ and C as $Li^+$ reacts with $CO_2$. The reversible charge process involves $Li_2CO_3$ decomposition into $Li^+$ and $CO_2$. Achieving long-term stable performance with low overpotential remains a challenge due to slow reaction kinetics. The utilization of $CO_2$ gas in Li–$CO_2$ batteries offers a promising solution, aligning with efforts to combat global warming and climate change. Therefore, Li–$CO_2$ batteries, utilizing $CO_2$ gas directly as a redox medium, represent a highly favorable energy storage system.[232–235] SAMs are pivotal in enhancing the $CO_2$ reduction process at the cathode of Li–$CO_2$ cells, significantly enhancing reaction kinetics. For instance, N-doped carbon nanotubes supporting atomically dispersed $IrO_x$/Ir bi-phase particles have been employed as SACs, enabling a reversible

Li–$CO_2$ reaction. This setup displays low overpotential and maintains stable cycling performance over 120 cycles (Figure 11k).[236] The SACs boost surface catalytic activities, while N-doped carbon nanotubes enhance electronic conductivity and provide favorable nucleation sites for Ir loading. This combination of SACs and N-doped carbon nanotubes demonstrates promising potential for promoting Li–$CO_2$ battery properties.[236] In another study, a catalyst, engineered with distinct Ru atomic clusters and composite single-atom Ru–$N_4$ sites supported on N-doped carbon (RuAC+SA@NCB),[237] enhances electrocatalytic performance for the C $CO_2$RR due to electronic synergy between RuAC and Ru–$N_4$ (Figure 11l). The electronic characteristics of the Ru–$N_4$ sites are fine-tuned by neighboring RuAC species, reducing energy barriers for rate-determining steps of the C $O_2$RR and CER. Full cell evaluations demonstrate remarkable performance with low overpotentials of 1.65 and 1.86 V at high rates of 1 and 2 A $g^{-1}$, respectively, along with an extended cycling lifespan compared to baseline catalysts (Figure 11m,n).[237] In addition to noble metal catalysis, other single-metal atom catalysts such as $Fe_1$/N-rGO, $Co_1$/N-rGO, and $Ni_1$/N-rGO, comprising iron, cobalt, and nickel anchored onto N-doped reduced graphene oxide, are studied for their catalytic property in $Li_2CO_3$ decomposition.[238] Particularly, $Fe_1$/N-rGO demonstrates remarkable performance with a discharge capacity of 16 835 mAh $g^{-1}$ at 100 mA $g^{-1}$ and excellent stability over 170 cycles.[238]

## 7. Conclusions and Perspectives

Overall, this review delves into the fields of SAMs and their potential impact on electronic energy storage technologies. Starting with an analysis of the advantages, challenges, and operational mechanisms of SAMs in energy storage systems, it proceeds to explore their specific applications. Their distinctive electronic and structural properties endow them with remarkable electrochemical storage and catalytic activity and selectivity, promising more efficient energy storage processes. With ongoing research, SAMs are poised to revolutionize electronic energy storage, contributing significantly to a sustainable and clean energy future. However, despite substantial advancements, further progress in these fields faces specific challenges.

(a) The scalability of synthesis methods and associated costs pose significant challenges for the widespread adoption of SAMs in energy storage technologies. Current synthesis techniques are intricate, requiring precise control and sophisticated equipment, hindering scalability. Optimizing existing synthesis methods to balance precision and scalability is essential, especially for high-loading SAMs. Researchers need to explore modifications or entirely new approaches to enable large-scale production without compromising quality. Besides, the choice of precursor materials significantly influences costs, necessitating the identification and utilization of more cost-effective sources without sacrificing quality. This may involve investigating alternative precursors or designing processes using readily available resources. Addressing these challenges will facilitate cost-effective and scalable production of SAMs, enhancing their integration into electronic energy storage technologies.

(b) Long-term stability and durability are critical for the practical implementation of SAMs in electronic energy storage applications. While these materials exhibit promising properties in controlled laboratory settings, their performance over extended periods and under real-world conditions requires further exploration. Understanding degradation mechanisms and how these materials evolve over time, especially during repeated charging and discharging cycles and exposure to various electrolytes and environmental factors, is crucial. Retaining electrochemical active sites is vital for sustained performance, requiring strategies to prevent aggregation or migration of single atoms during cycling. This involves designing materials with stronger binding forces and optimizing synthesis methods for secure anchoring.

(c) Despite their remarkable properties, effectively integrating SAMs into current energy storage technologies faces significant challenges. Transitioning from laboratory-scale innovations to scalable, commercially viable applications is pivotal for widespread adoption. Compatibility with a range of electrochemical systems, including multiple chemistries and configurations, must be ensured to support widespread adoption. Understanding their interaction with different system components, such as electrolytes and electrode interactions, is vital for seamless integration. Overcoming these challenges requires a holistic approach encompassing scientific, technical, and economic considerations to ensure successful and sustainable adoption in practical applications.

(d) Understanding the intricate behaviors and mechanisms of SAMs in energy storage is a multifaceted challenge. SAMs interact with electrolytes, substrates, and external conditions, making it challenging to predict and control their dynamic behavior. To address this challenge, employing advanced characterization techniques, such as in situ or operando spectroscopy, microscopy, and computational modeling, becomes imperative. These techniques offer real-time insights into SAMs' structural transformations, reaction intermediates at atomic and molecular levels, and a dynamic perspective, capturing transient phenomena and enhancing our understanding of SAMs' responses under practical operating conditions. The integration of experimental findings with computational simulations bridges the gap between real-world observations and theoretical predictions. Adopting a multi-scale modeling approach considers SAMs' behavior at different length and time scales, connecting atomic interactions with macroscopic performance. In summary, a strategic and integrated approach combining experimental techniques and computational modeling is vital for optimizing SAMs' performance in energy applications.

(e) As for the materials design, several promising future directions can be envisioned to further enhance the functionality and applicability of SAMs in advanced energy storage systems. First, the rational design of multifunctional SAMs capable of simultaneously regulating interfacial chemistry, ion transport, and reaction kinetics will be essential for addressing the multi-faceted challenges inherent to complex electrochemical reactions. Such designs may incorporate dual-function coordination environments or synergistic host–guest interactions to facilitate selective

adsorption and accelerated redox pathways. Besides, the integration of SAMs with 2D materials (e.g., MXenes, graphene, TMDs) or hybrid organic–inorganic frameworks may lead to hierarchical architectures that not only maximize atom utilization but also enhance charge transfer, ion diffusion, and active site accessibility. These composite systems could serve as modular building blocks for next-generation electrode designs with improved scalability, processability, and performance. These directions highlight the pivotal role of materials innovation in pushing the boundaries of single-atom engineering for electrochemical energy technologies.

While the potential of SAMs in energy storage is promising, ensuring scalability, long-term stability, and seamless integration with existing technologies is crucial for their successful application. Future research endeavors should prioritize the development of scalable and cost-effective synthesis methods, enhance the durability of SAMs, and focus on seamless integration into practical energy storage devices. These efforts will unlock the full potential of SAMs, advancing sustainable and efficient energy technologies.

## Acknowledgements

J.G. and Y.R. contributed equally to this work. This work was supported by the King Abdullah University of Science and Technology, the Center of Excellence for Renewable Energy and Storage Technologies under award number 5937, the KAUST Supercomputing Laboratory under project k10175, and the National Natural Science Foundation of China (Grant no. 52102203).

## Conflict of Interest

The authors declare no conflict of interest.

## Keywords

energy conversion, energy storage, real application, single atom materials

Received: March 14, 2025
Revised: June 18, 2025
Published online:

[1] Y. Guo, W. Zhao, D. Li, J. Liu, J. Qian, L. Pang, T. Zhou, W. Liu, Z. Liu, H. Huang, J. Zhai, D. Zhou, *Adv. Mater.* **2024**, *37*, 2415652.
[2] X. Tian, C. Ye, L. Zhang, M. K. Sugumar, Y. Zhao, N. B. McKeown, S. Margadonna, R. Tan, *Adv. Mater.* **2024**, *37*, 2402335.
[3] A. Kingan, C. Huang, Z. R. Mansley, R. C. Hill, Z. Wang, D. C. Bock, L. Wang, L. Ma, S. N. Ehrlich, J. Bai, H. Zhong, C. Jaye, C. Weiland, A. C. Marschilok, E. S. Takeuchi, Y. Zhu, S. Yan, K. J. Takeuchi, *ACS Nano* **2024**, *18*, 34776.
[4] S. Qian, X. Tan, Y. Zhu, Y. Wang, H. Chen, M. Zheng, C. Zhang, S. Zhang, J. Lu, *ACS Nano* **2024**, *18*, 34363.
[5] Y. Wang, W. Li, C. Huang, Z. Jiang, F. Liu, X. Zhou, W. Zhang, W. Zheng, *Adv. Funct. Mater.* **2024**, *35*, 2420580.
[6] Z. Zhao, W. Liu, T. Kong, Y. Liu, W. Chen, P. Gao, D. Bi, *Adv. Funct. Mater.* **2024**, *35*, 2419393.
[7] M. Liu, L.-J. Hu, Z.-K. Guan, T.-L. Chen, X.-Y. Zhang, S. Sun, R. Shi, P. Jing, P.-F. Wang, *Nano-Micro Lett.* **2025**, *17*, 85.
[8] I. Kim, S. Kim, H. Cho, J. Jung, H. Kwon, D. Kim, Y. Shin, H.-T. Kim, *Adv. Energy Mater.* **2024**, *15*, 2403828.
[9] M. M. Nishshanke, P. Jovanovic, M. R. Panda, M. J. Abedin, D. McNamara, M. R. Hill, J. Bhattacharya, C. Kamal, M. Shaibani, M. Majumder, *Adv. Energy Mater.* **2024**, *15*, 2403092.
[10] M. Huang, L. Song, N. Wang, Y. Fu, R. Ren, Z. Li, Y. Lu, J. Xu, Q. Liu, *Angew. Chem., Int. Ed.* **2024**, *64*, 202414893.
[11] Y. Rao, J. Yang, J. Tian, W. Ning, S. Guo, H. Zhou, *Angew. Chem., Int. Ed.* **2024**, *64*, 202418893.
[12] F. Zhang, Z. Hu, J. Lai, A. Faiza, X. Hu, W. Sun, A. Zhou, H. Wang, Y. Chen, T. Xue, Y. Ye, N. Chen, L. Li, F. Wu, R. Chen, *Angew. Chem., Int. Ed.* **2024**, *136*, 202412035.
[13] Y. Liu, P. Shu, M. Zhang, B. Chen, Y. Song, B. Lu, R. Mao, Q. Peng, G. Zhou, H.-M. Cheng, *ACS Energy Lett.* **2024**, *9*, 2173.
[14] J. Zou, G. Liang, J. A. Yuwono, F. Zhang, Y. Fan, S. Zhang, B. Johannessen, L. Sun, Z. Guo, *ACS Energy Lett.* **2024**, *9*, 5145.
[15] Y. Chen, J. Li, B. Lu, Y. Liu, R. Mao, Y. Song, H. Li, X. Yu, Y. Gao, Q. Peng, X. Qi, G. Zhou, *Adv. Mater.* **2024**, *36*, 2406856.
[16] Y. Liu, X. Wu, H. Qu, G. Lu, Y. Chen, B. Lu, Y. Song, G. Zhou, H.-M. Cheng, *Adv. Mater.* **2024**, *37*, 2411652.
[17] S. C. Sand, J. L. M. Rupp, B. Yildiz, *Chem. Soc. Rev.* **2024**, *54*, 178.
[18] N. Kitchamsetti, C. K. Mannem, C. S. Chakra, A. L. F. de Barros, *J. Energy Storage* **2025**, *106*, 114836.
[19] S. Maiti, M. T. Curnan, K. Kim, K. Maiti, J. K. Kim, *Adv. Energy Mater.* **2024**, *14*, 2401911.
[20] J. Zou, L. Tang, W. He, X. Zhang, *ACS Nano* **2024**, *18*, 34492.
[21] B. Mortazavi, *Adv. Energy Mater.* **2024**, *15*, 2403876.
[22] M. Zhou, X. Huang, H. Li, X. Duan, Q. Zhao, T. Ma, *Angew. Chem., Int. Ed.* **2024**, *63*, 202413354.
[23] Q. L. Wang, H. W. Wang, H. Cao, C. W. Tung, W. Liu, S. F. Hung, W. J. Wang, C. Zhu, Z. H. Zhang, W. Z. Cai, Y. Q. Cheng, H. B. Tao, H. M. Chen, Y. G. Wang, Y. J. Li, H. B. Yang, Y. Q. Huang, J. Li, B. Liu, *Nat. Catal.* **2023**, *6*, 916.
[24] K. Sun, J. C. Dong, H. Sun, X. D. Wang, J. J. Fang, Z. B. Zhuang, S. B. Tian, X. M. Sun, *Nat. Catal.* **2023**, *6*, 1164.
[25] H. Kang, L. Zhu, S. Y. Li, S. W. Yu, Y. M. Niu, B. S. Zhang, W. Chu, X. C. Liu, S. Perathoner, G. Centi, Y. F. Liu, *Nat. Catal.* **2023**, *6*, 1062.
[26] Y. Q. Huang, B. Liu, *Nat. Energy* **2023**, *8*, 577.
[27] H. Y. Fang, H. Mahalingam, X. Z. Li, X. Han, Z. Z. Qiu, Y. X. Han, K. Noori, D. Dulal, H. F. Chen, P. Lyu, T. H. Yang, J. Li, C. L. Su, W. Chen, Y. Q. Cai, A. H. C. Neto, K. S. Novoselov, A. Rodin, J. Lu, *Nat. Nanotechnol.* **2023**, *18*, 1401.
[28] Y. Li, Y. Zeng, Y. Chen, D. Luan, S. Gao, X. W. Lou, *Angew. Chem., Int. Ed.* **2022**, *61*, 202212680.
[29] C. Zhao, G.-L. Xu, Z. Yu, L. Zhang, I. Hwang, Y.-X. Mo, Y. Ren, L. Cheng, C.-J. Sun, Y. Ren, *Nat. Nanotechnol.* **2021**, *16*, 166.
[30] X. Hu, G. Luo, Q. Zhao, D. Wu, T. Yang, J. Wen, R. Wang, C. Xu, N. Hu, *J. Am. Chem. Soc.* **2020**, *142*, 16776.
[31] S. Kment, A. Bakandritsos, I. Tantis, H. Kmentová, Y. Zuo, O. Henrotte, A. Naldoni, M. Otyepka, R. S. Varma, R. Zbořil, *Chem. Rev.* **2024**, *124*, 11767.
[32] Y. Wu, X. C. Wang, F. Zhang, L. J. Hai, Q. H. Chen, C. Q. Chao, A. K. Yang, Y. Sun, D. Z. Jia, *Adv. Funct. Mater.* **2023**, *34*, 2309552.
[33] Y. Wang, A. Outka, W. M. Takele, M. Avdeev, S. Sainio, R. Liu, V. Kee, W. Choe, B. Raji-Adefila, D. Nordlund, S. Zhou, W. H. Kan, T. G. Habteyes, D. C. Chen, *Adv. Mater.* **2023**, *35*, 2306396.
[34] J. Ma, T. T. Liu, J. Ma, C. Zhang, J. H. Yang, *Adv. Sci.* **2023**, *11*, 2304938.
[35] Z. H. Cui, Z. Z. Guo, A. Manthiram, *Angew. Chem., Int. Ed.* **2023**, *62*, 202313437.

[36] J. Q. Zhu, Z. Cui, H. Wang, L. J. Zhang, Q. Liu, A. J. Lu, T. Ji, J. Q. Hu, W. Luo, R. J. Zou, *Adv. Energy Mater.* **2023**, *13*, 2302687.
[37] C. Shen, L. B. Hu, Q. M. Duan, X. Y. Liu, S. S. Huang, Y. Jiang, W. R. Li, B. Zhao, X. L. Sun, J. J. Zhang, *Adv. Energy Mater.* **2023**, *13*, 2302957.
[38] M. Kubot, L. Balke, J. Scholz, S. Wiemers-Meyer, U. Karst, H. Hayen, H. Hur, M. Winter, J. Kasnatscheew, S. Nowak, *Adv. Sci.* **2023**, *11*, 2305282.
[39] J. F. Baumgärtner, M. Wörle, C. P. Guntlin, F. Krumeich, S. Siegrist, V. Vogt, D. C. Stoian, D. Chernyshov, W. van Beek, K. V. Kravchyk, M. V. Kovalenko, *Adv. Mater.* **2023**, *35*, 2304158.
[40] X. T. Yang, Y. Gao, L. Fan, A. M. Rao, J. Zhou, B. A. Lu, *Adv. Energy Mater.* **2023**, *13*, 2302589.
[41] X. M. Ma, H. W. Fu, J. Y. Shen, D. W. Zhang, J. W. Zhou, C. Y. Tong, A. M. Rao, J. Zhou, L. Fan, B. A. Lu, *Angew. Chem., Int. Ed.* **2023**, *62*, 202312973.
[42] W. B. Jian, X. Q. Qiu, Y. Y. Lai, P. C. Yin, J. X. Lin, W. L. Zhang, *Adv. Energy Mater.* **2023**, *13*, 2301303.
[43] C. L. Chi, Z. Liu, G. W. Wang, B. Qi, Z. P. Qiu, Y. C. Yan, C. Huangfu, X. L. Lu, X. H. Yang, M. Gong, K. Cao, T. Wei, Z. J. Fan, *Adv. Energy Mater.* **2023**, *13*, 2302055.
[44] Y. Zong, H. C. Chen, J. S. Wang, M. H. Wu, Y. Chen, L. Y. Wang, X. L. Huang, H. W. He, X. Ning, Z. C. Bai, W. Wen, D. M. Zhu, X. C. Ren, N. N. Wang, S. X. Dou, *Adv. Mater.* **2023**, *35*, 2306269.
[45] Y. Li, Z. Q. Pang, A. Ghani, J. M. Little, L. P. Wang, H. C. Yang, Y. S. Zhao, P. Y. Chen, *Adv. Energy Mater.* **2023**, *13*, 2301557.
[46] Z. Y. Jiao, X. X. Cai, X. X. Wang, Y. R. Li, Z. Bie, W. X. Song, *Adv. Energy Mater.* **2023**, *13*, 2302676.
[47] K. Du, Y. J. Liu, Y. F. Yang, F. Y. Cui, J. S. Wang, M. S. Han, J. W. Su, J. J. Wang, X. P. Han, Y. X. Hu, *Adv. Mater.* **2023**, *35*, 2301538.
[48] L. Ma, Y. Q. Zhang, S. Zhang, L. Wang, C. X. Zhang, Y. J. Chen, Q. Wu, L. B. Chen, L. J. Zhou, W. F. Wei, *Adv. Funct. Mater.* **2023**, *33*, 2305788.
[49] Z. Li, Y. Li, C. X. Bi, Q. K. Zhang, L. P. Hou, X. Y. Li, J. Ma, X. Q. Zhang, B. Q. Li, R. Wen, Q. Zhang, *Adv. Funct. Mater.* **2023**, *34*, 2304541.
[50] Y. A. Li, Y. R. Deng, J. L. Yang, W. H. Tang, B. Ge, R. P. Liu, *Adv. Funct. Mater.* **2023**, *33*, 2302267.
[51] C. Huang, J. Yu, C. Li, Z. B. Cui, C. Q. Zhang, C. Y. Zhang, B. F. Nan, J. S. Li, J. Arbiol, A. Cabot, *Adv. Funct. Mater.* **2023**, *33*, 2305624.
[52] C. L. Miao, X. X. Wang, D. H. Guan, J. X. Li, H. F. Wang, J. J. Xu, *Adv. Funct. Mater.* **2023**, *34*, 2307150.
[53] Z. J. Zhang, X. Xiao, W. T. Yu, Z. X. Zhao, P. Tan, *Nano Lett.* **2022**, *22*, 7527.
[54] C. Prehal, S. Mondal, L. Lovicar, S. A. Freunberger, *ACS Energy Lett.* **2022**, *7*, 3112.
[55] H. Kim, K. J. Min, M. G. Jeong, H. G. Jung, Y. K. Sun, *ACS Appl. Mater. Interfaces* **2022**, *14*, 45945.
[56] J. S. Zou, G. M. Liang, F. L. Zhang, S. L. Zhang, K. Davey, Z. P. Guo, *Adv. Mater.* **2023**, *35*, 2210671.
[57] Y. L. Wu, H. X. Li, T. C. Liu, M. Xu, *Adv. Mater.* **2023**, *35*, 2305063.
[58] C. H. Wu, G. C. Qi, J. X. Zhang, J. L. Cheng, B. Wang, *Small* **2023**, *19*, 2302078.
[59] J. D. Wang, B. Marchetti, X. D. Zhou, S. Y. Wei, *ACS Energy Lett.* **2023**, *8*, 1818.
[60] Z. B. Cheng, Y. L. Fang, Y. S. Yang, H. Zhang, Z. W. Fan, J. D. Zhang, S. C. Xiang, B. L. Chen, Z. J. Zhang, *Angew. Chem., Int. Ed.* **2023**, *135*, 202311480.
[61] J. X. Yu, M. C. Jiang, W. Zhang, G. Li, R. A. Soomro, N. Sun, B. Xu, *Small Methods* **2023**, *7*, 2300708.
[62] K. K. Yang, W. Zhou, Q. F. Fu, L. L. Xiao, Y. Mo, J. L. Ke, W. Z. Shen, Z. Y. Wang, J. Tu, S. Chen, P. Gao, J. L. Liu, *Adv. Funct. Mater.* **2023**, *33*, 2306190.
[63] H. Liu, M. Y. Cheng, Z. C. Tian, L. M. Cui, D. Wu, D. X. Wang, L. Zhou, J. L. Xia, *Adv. Funct. Mater.* **2023**, *33*, 2306424.
[64] N. Huang, C. Tang, H. Jiang, J. Sun, A. J. Du, H. J. Zhang, *Nano Res.* **2023**, *17*, 2619.
[65] R. Razaq, M. M. U. Din, D. R. Småbråten, V. Eyupoglu, S. Janakiram, T. O. Sunde, N. Allahgoli, D. Rettenwander, L. Y. Deng, *Adv. Energy Mater.* **2023**, *14*, 2302897.
[66] X. He, K. Zhang, Z. Q. Zhu, Z. F. Tong, X. Liang, *Chem. Soc. Rev.* **2023**, *53*, 9.
[67] S. M. Chai, Y. Zhong, Y. J. Wang, Q. He, A. Azizi, L. Y. Chen, X. T. Ren, W. F. Wei, S. Q. Liang, Z. Chang, A. Q. Pan, *Adv. Energy Mater.* **2023**, *14*, 2303020.
[68] W. Xiao, K. Yoo, J. H. Kim, H. Y. Xu, *Adv. Sci.* **2023**, *10*, 2303916.
[69] J. Liu, Y. H. Zhou, T. Y. Yan, X. P. Gao, *Adv. Funct. Mater.* **2023**, *34*, 2309625.
[70] H. Li, H. X. Yang, X. P. Ai, *Adv. Mater.* **2023**, 2305038.
[71] Z. Y. Han, R. H. Gao, T. S. Wang, S. Y. Tao, Y. Y. Jia, Z. J. Lao, M. T. Zhang, J. Q. Zhou, C. Li, Z. H. Piao, X. Zhang, G. M. Zhou, *Nat. Catal.* **2023**, *6*, 1073.
[72] P. Zhu, W. Y. Feng, D. Zhao, P. Y. Song, M. W. Li, X. Tan, T. Liu, S. J. Liu, W. Zhu, Z. B. Zhuang, J. T. Zhang, C. Chen, *Angew. Chem., Int. Ed.* **2023**, *135*, 202304488.
[73] B. Y. Huang, X. N. Tang, Y. S. Hong, L. B. Li, T. Hu, K. Yuan, Y. W. Chen, *Angew. Chem., Int. Ed.* **2023**, *135*, 202306667.
[74] A. L. Han, W. M. Sun, X. Wan, D. D. Cai, X. J. Wang, F. Li, J. L. Shui, D. S. Wang, *Angew. Chem., Int. Ed.* **2023**, *62*, 202303185.
[75] N. K. Guo, H. Xue, R. Ren, J. Sun, T. S. Song, H. L. Dong, Z. L. Zhao, J. W. Zhang, Q. Wang, L. M. Wu, *Angew. Chem., Int. Ed.* **2023**, *62*, 202312409.
[76] W. X. Zou, Y. Y. Cheng, Y. X. Ye, X. Q. Wei, Q. Tong, L. Dong, G. F. Ouyang, *Angew. Chem., Int. Ed.* **2023**, *62*, 202313392.
[77] Y. C. Xiong, Y. H. Wang, J. W. Zhou, F. Liu, F. K. Hao, Z. X. Fan, *Adv. Mater.* **2023**, *36*, 2304021.
[78] W. Q. Song, C. X. Xiao, J. Ding, Z. C. Huang, X. Y. Yang, T. Zhang, D. Mitlin, W. B. Hu, *Adv. Mater.* **2023**, *36*, 2301477.
[79] Y. C. Li, E. P. Delmo, G. Y. Hou, X. L. Cui, M. Zhao, Z. H. Tian, Y. Zhang, M. H. Shao, *Angew. Chem., Int. Ed.* **2023**, *62*, 202313522.
[80] D. Lin, Y. Liu, Z. Liang, H.-W. Lee, J. Sun, H. Wang, K. Yan, J. Xie, Y. Cui, *Nat. Nanotechnol.* **2016**, *11*, 626.
[81] Y. Li, S. Lin, D. Wang, T. Gao, J. Song, P. Zhou, Z. Xu, Z. Yang, N. Xiao, S. Guo, *Adv. Mater.* **2020**, *32*, 1906722.
[82] J. Gu, Q. Zhu, Y. Shi, H. Chen, D. Zhang, Z. Du, S. Yang, *ACS Nano* **2020**, *14*, 891.
[83] L. Zhang, D. Liu, Z. Muhammad, F. Wan, W. Xie, Y. Wang, L. Song, Z. Niu, J. Chen, *Adv. Mater.* **2019**, *31*, 1903955.
[84] T. Yang, T. Qian, Y. Sun, J. Zhong, F. Rosei, C. Yan, *Nano Lett.* **2019**, *19*, 7827.
[85] P. Liu, L. C. Miao, Z. Q. Sun, X. C. Chen, Y. C. Si, Q. L. Wang, L. F. Jiao, *Angew. Chem., Int. Ed.* **2023**, *135*, 202312413.
[86] Q. Zhang, Y. K. Li, E. T. Poh, Z. X. Xing, M. S. Zhang, M. Wang, Z. J. Sun, J. S. Pan, S. V. C. Vummaleti, J. Zhang, W. Chen, *Adv. Energy Mater.* **2023**, *13*, 2301748.
[87] X. Guo, H. Xu, W. Li, Y. Liu, Y. Shi, Q. Li, H. Pang, *Adv. Sci.* **2023**, *10*, 2206084.
[88] Z. Yi, S. Jiang, J. Tian, Y. Qian, S. Chen, S. Wei, N. Lin, Y. Qian, *Angew. Chem., Int. Ed.* **2020**, *59*, 6459.
[89] T. Li, D. Yu, J. Liu, F. Wang, *ACS Appl. Mater. Interfaces* **2019**, *11*, 37559.
[90] C. Wei, M. Tian, Z. Fan, L. Yu, Y. Song, X. Yang, Z. Shi, M. Wang, R. Yang, J. Sun, *Energy Storage Mater.* **2021**, *41*, 141.
[91] L. Lv, Z. Yang, K. Chen, C. Wang, Y. Xiong, *Adv. Energy Mater.* **2019**, *9*, 1803358.
[92] S. Chen, Z. Kang, X. Hu, X. Zhang, H. Wang, J. Xie, X. Zheng, W. Yan, B. Pan, Y. Xie, *Adv. Mater.* **2017**, *29*, 1701687.
[93] W. Zhang, Y. H. Dai, R. W. Chen, Z. M. Xu, J. W. Li, W. Zong, H. X. Li, Z. Li, Z. Y. Zhang, J. X. Zhu, F. Guo, X. Gao, Z. J. Du, J. T. Chen,

T. L. Wang, G. J. He, I. P. Parkin, *Angew. Chem., Int. Ed.* **2022**, *62*, 202212695.
[94] L. Han, Q. Wang, R. Pang, D. Zhang, B. Zhao, W. X. Meng, M. Li, Y. J. Zhang, A. Y. Cao, Y. Y. Shang, *Adv. Energy Mater.* **2023**, *13*, 2302395.
[95] B. F. Zhang, L. X. He, R. L. Zhang, W. Yuan, J. Wang, Y. X. Hu, Z. H. Zhao, L. L. Zhou, J. Wang, Z. L. Wang, *Adv. Energy Mater.* **2023**, *13*, 2301353.
[96] Z. M. Liang, Y. Y. Wang, B. Pei, S. B. Son, M. Nguyen, N. R. Singstock, S. F. Huang, M. C. Mo, J. L. Li, M. S. Whittingham, C. M. Ban, *Adv. Energy Mater.* **2023**, *13*, 2301295.
[97] K. J. Jun, L. Kaufman, W. M. Jung, B. Park, C. Jo, T. Yoo, D. H. Lee, B. J. Lee, B. D. McCloskey, H. Kim, G. Ceder, *Adv. Energy Mater.* **2023**, *13*, 2301132.
[98] D. Igarashi, Y. Tanaka, K. Kubota, R. Tatara, H. Maejima, T. Hosaka, S. Komaba, *Adv. Energy Mater.* **2023**, *13*, 2302647.
[99] S. Fan, S. Cui, J. Zhang, J. Rong, W. Wang, X. Xing, Y. Liu, W. Ma, J.-T. Zhao, *Small* **2023**, *19*, 2304290.
[100] S. Cui, J. Zhang, S. Fan, X. Xing, L. Deng, Y. Gong, *Nano Lett.* **2022**, *22*, 9559.
[101] J. Zhang, E. Wang, S. Cui, S. Yang, X. Zou, Y. Gong, *Nano Lett.* **2022**, *22*, 1398.
[102] Q. Li, M. Yuan, Y. Ji, X. Chen, Y. Wang, X. Gao, H. Li, H. He, H. Chen, Q. Tan, *Chem. Eng. J.* **2022**, *437*, 135340.
[103] H.-e. Kim, S. Jang, H. Lim, W. Chung, I. Nam, J. H. Bang, *Appl. Surf. Sci.* **2023**, *624*, 157161.
[104] S. Liu, Z. Lin, F. Xiao, J. Zhang, D. Wang, X. Chen, Y. Zhao, J. Xu, *Chem. Eng. J.* **2020**, *389*, 124377.
[105] Z. Wen, Y. Chen, D. Hu, B. He, M. Zhou, *New J. Chem.* **2023**, *47*, 5659.
[106] B. Sun, W. Zheng, B. Xie, C. Kang, J. Zhu, F. Kong, L. Xiang, C. Cui, S. Lou, C. Du, P. Zuo, J. Xie, G. Yin, *Small* **2022**, *18*, 2200367.
[107] K. Sada, J. Darga, A. Manthiram, *Adv. Energy Mater.* **2023**, *13*, 2302321.
[108] Z. X. Li, L. H. Yu, X. Tao, Y. Li, L. L. Zhang, X. D. He, Y. Chen, S. Xiong, W. Hu, J. Li, J. C. Wang, H. L. Jin, S. Wang, *Small* **2023**, *2304124*, 2304124.
[109] A. Joshi, S. Chakrabarty, S. H. Akella, A. Saha, A. Mukherjee, B. Schmerling, M. Ejgenberg, R. Sharma, M. Noked, *Adv. Mater.* **2023**, *35*, 2304440.
[110] Z. Lu, J. Wang, W. Feng, X. Yin, X. Feng, S. Zhao, C. Li, R. Wang, Q. A. Huang, Y. Zhao, *Adv. Mater.* **2023**, *35*, 2211461.
[111] X. Hu, G. Wang, J. Li, J. Huang, Y. Liu, G. Zhong, J. Yuan, H. Zhan, Z. Wen, *Energy Environ. Sci.* **2021**, *14*, 4564.
[112] C. Wang, B. Li, W. Shen, F. Kang, Z. H. Huang, R. Lv, *Adv. Funct. Mater.* **2023**, *33*, 2214429.
[113] Y. F. Liu, Y. T. Shi, C. T. Gao, Z. D. Shi, H. B. Ding, Y. H. Feng, Y. M. He, J. W. Sha, J. Zhou, B. A. Lu, *Angew. Chem., Int. Ed.* **2023**, *62*, 202300016.
[114] B. Xiao, Z. Sun, H. Zhang, Y. Wu, J. Li, J. Cui, J. Han, M. Li, H. Zheng, J. Chen, *Energy Environ. Sci.* **2023**, *16*, 2153.
[115] F. Liu, J. Meng, G. Jiang, J. Li, H. Wang, Z. Xiao, R. Yu, L. Mai, J. Wu, *Matter* **2021**, *4*, 4006.
[116] D. Yu, W. Luo, H. Gu, K. Li, J. Liang, H. Chen, Q. Wang, D. Chen, Y. Huang, P. Novikov, *Chem. Eng. J.* **2023**, *454*, 139908.
[117] Y. Chen, N. Fu, B. Shen, Y. Yan, W. Shao, T. Wang, H. Xie, Z. Yang, *Small* **2023**, *19*, 2207423.
[118] X. Guo, H. Gao, S. Wang, G. Yang, X. Zhang, J. Zhang, H. Liu, G. Wang, *Nano Lett.* **2022**, *22*, 1225.
[119] L. L. Zhang, Y. N. Chen, Z. Y. Jiang, J. W. Chen, C. Wei, W. Z. Wu, S. H. Li, Q. Xu, *Energy Environ. Mater.* **2023**, *7*, 12507.
[120] Z. Q. Wang, J. F. Diao, J. N. Burrow, K. K. Reimund, N. Katyal, G. Henkelman, C. B. Mullins, *Adv. Funct. Mater.* **2023**, *33*, 2304791.
[121] X. Y. Meng, S. Zhou, J. W. Li, Y. N. Chen, S. Y. Lin, C. Han, A. Q. Pan, *Adv. Funct. Mater.* **2023**, *34*, 2309350.
[122] W. G. Lim, X. L. Li, D. Reed, *Small Methods* **2023**, *8*, 2300965.
[123] Z. Zhang, S. Li, X. Wang, Z. Wen, J. Sun, *J. Phys. Chem. C* **2021**, *125*, 26371.
[124] P. Sharma, M. M. Sundaram, T. Watcharatharapong, D. Laird, H. Euchner, R. Ahuja, *ACS Appl. Mater. Interfaces* **2020**, *12*, 44815.
[125] H. Yi, A. Gao, X. Pang, Z. Ao, D. Shu, S. Deng, F. Yi, C. He, X. Zhou, Z. Zhu, *ACS Appl. Energy Mater.* **2020**, *3*, 10192.
[126] Z. Li, D. Wang, H. Li, M. Ma, Y. Zhang, Z. Yan, S. Agnoli, G. Zhang, X. Sun, *Nano Res.* **2022**, *15*, 1715.
[127] L. Yang, P. Liu, J. Zhou, *ACS Appl. Energy Mater.* **2023**, *6*, 10105.
[128] P. Li, C. Zhu, L. Yang, J. Shi, W. Hu, Z. Li, J. Wu, H. Wang, *Energy Storage Mater.* **2024**, *71*, 103639.
[129] N. Nwaji, G. M. Zewdie, J. Gwak, H. Kang, L. T. Tufa, Y. Choi, M. Goddati, H. Shin, J. Lee, *J. Energy Storage* **2024**, *83*, 110671.
[130] P. Pal, S. Bhowmik, M. Nandi, *Chem.-Eur. J.* **2024**, *30*, 202400638.
[131] Q. Rong, C. Yuwen, Y. Liu, Y. Liu, C. Wang, Y. Wang, D. Zhang, Z. Wen, *Nano Res.* **2024**, *17*, 4039.
[132] K. Zhang, Z. Wu, Z. Yang, J. Sun, C. Ma, S. Luo, W. Li, S. Liu, *J. Energy Storage* **2024**, *95*, 112395.
[133] N. Zhu, Y. X. Yang, Y. Li, Y. Bai, J. F. Rong, C. Wu, *Carbon Energy* **2023**, *6*, 423.
[134] S. Z. Fan, S. Q. Cui, J. J. Zhang, J. S. Rong, W. X. Wang, X. T. Xing, Y. R. Liu, W. W. Ma, J. T. Zhao, *Small* **2023**, *19*, 2304290.
[135] C. H. Zhang, T. Jin, J. D. Liu, J. M. Ma, N. W. Li, L. Yu, *Small* **2023**, *19*, 2301523.
[136] X. C. Wang, Y. F. He, S. Y. Liu, Y. J. Li, S. B. Tu, R. M. Zhan, Z. H. Chen, J. J. Fu, Z. Cai, L. Wang, Y. M. Sun, *Adv. Funct. Mater.* **2023**, *33*, 2307281.
[137] Y. S. Feng, Y. N. Li, P. Wang, Z. P. Guo, F. F. Cao, H. Ye, *Angew. Chem., Int. Ed.* **2023**, *62*, 202310132.
[138] T. Wei, Y. Y. Zhou, C. Sun, X. T. Guo, S. D. Xu, D. F. Chen, Y. F. Tang, *Nano Res.* **2023**, *17*, 2763.
[139] G. Q. Peng, Q. F. Zheng, G. Luo, D. W. Zheng, S. P. Feng, U. Khan, A. R. Akbar, H. M. Luo, F. D. Liu, *Small* **2023**, *19*, 2303787.
[140] J. Y. Ding, Y. C. Wen, X. X. Lan, R. Z. Hu, *ACS Appl. Mater. Interfaces* **2023**, *15*, 6768.
[141] H. B. Chen, J. Hu, H. Li, J. L. Zhang, Q. Chen, G. Y. Hou, Y. P. Tang, *Small* **2023**, *20*, 2307598.
[142] K. Xu, M. Zhu, X. Wu, J. Liang, Y. Liu, T. Zhang, Y. Zhu, Y. Qian, *Energy Storage Mater.* **2019**, *23*, 587.
[143] Y. Sun, J. Zhou, H. Ji, J. Liu, T. Qian, C. Yan, *ACS Appl. Mater. Interfaces* **2019**, *11*, 32008.
[144] S. Haodong, L. Yaguang, L. Pengfei, W. Zhong-Shuai, *Acta Phys.-Chim. Sin.* **2021**, *37*, 2008033.
[145] Y. Li, D. Fang, X. L. Li, D. Yan, S. Xi, T. C. Li, C. Lin, S. Huang, J. Qiu, X. Xu, *Energy Environ. Mater.* **2023**, *6*, 12449.
[146] S. A. Wu, J. Hwang, K. Matsumoto, R. Hagiwara, *Adv. Energy Mater.* **2023**, *13*, 2302468.
[147] S. Y. Wang, S. T. Weng, X. P. Li, Y. Liu, X. L. Huang, Y. L. Jie, Y. X. Pan, H. M. Zhou, S. H. Jiao, Q. Li, X. F. Wang, T. Cheng, R. G. Cao, D. S. Xu, *Angew. Chem., Int. Ed.* **2023**, *135*, 202313447.
[148] Z. M. Ding, Y. S. Tang, T. Ortmann, J. K. Eckhardt, Y. T. Dai, M. Rohnke, G. Melinte, C. Heiliger, J. Janek, C. Kübel, *Adv. Energy Mater.* **2023**, *13*, 2302322.
[149] X. Li, W. Ye, P. Xu, H. Huang, J. Fan, R. Yuan, M. S. Zheng, M. S. Wang, Q. Dong, *Adv. Mater.* **2022**, *34*, 2202898.
[150] E. Zhang, X. Hu, L. Meng, M. Qiu, J. Chen, Y. Liu, G. Liu, Z. Zhuang, X. Zheng, L. Zheng, *J. Am. Chem. Soc.* **2022**, *144*, 18995.
[151] Y. Z. Huang, L. Lin, Y. G. Zhang, L. Liu, B. Sa, J. Lin, L. S. Wang, D. L. Peng, Q. S. Xie, *Nano-Micro Lett.* **2023**, *15*, 67.
[152] H. Liu, X. Chen, X. B. Cheng, B. Q. Li, R. Zhang, B. Wang, X. Chen, Q. Zhang, *Small Methods* **2019**, *3*, 1800354.
[153] W. Huang, S. Liu, R. Yu, L. Zhou, Z. Liu, L. Mai, *Energy Environ. Mater.* **2023**, *6*, 12466.

[154] Z. Liang, C. Peng, J. Shen, Y. Yang, S. Yao, D. Xue, M. Zhu, J. Liu, *J. Power Sources* **2023**, *556*, 232474.
[155] Z. Yang, Y. Dang, P. Zhai, Y. Wei, Q. Chen, J. Zuo, X. Gu, Y. Yao, X. Wang, F. Zhao, *Adv. Energy Mater.* **2022**, *12*, 2103368.
[156] F. Zhang, X. C. Wang, M. M. Wu, A. K. Yang, Y. D. Li, M. Q. Man, Y. Li, J. X. Guo, *ACS Energy Lett.* **2023**, *8*, 4895.
[157] H. L. Yu, D. C. Jiang, X. L. Cheng, P. Lu, S. K. Li, H. Zhang, Y. Jiang, F. Z. Huang, *Adv. Funct. Mater.* **2023**, *33*, 2307628.
[158] S. F. Ye, N. Yao, X. Chen, M. Z. Ma, L. F. Wang, Z. H. Chen, Y. Yao, Q. Zhang, Y. Yu, *Angew. Chem., Int. Ed.* **2023**, *62*, 202307728.
[159] P. Gao, F. Zhang, X. C. Wang, M. M. Wu, Q. Xiang, A. K. Yang, Y. Sun, J. X. Guo, Y. D. Huang, *ACS Nano* **2023**, *17*, 20325.
[160] D. Zhang, X. Ma, L. Wu, J. Wen, F. Li, J. Zhou, A. M. Rao, B. Lu, *Adv. Energy Mater.* **2023**, *13*, 2203277.
[161] J. Cui, B. Jin, A. Xu, J. Li, M. Shao, *Adv. Sci.* **2023**, *10*, 2206479.
[162] X. T. Xie, J. B. Chen, X. Y. Chen, Z. C. Shi, *J. Electroanal. Chem.* **2023**, *949*, 117862.
[163] Y. Wu, C. Wang, C. J. Wang, Y. Zhang, J. B. Liu, Y. H. Jin, H. Wang, Q. Q. Zhang, *Mater. Horiz.* **2023**, *11*, 388.
[164] T. Naren, R. H. Jiang, G. C. Kuang, L. J. Zhou, L. B. Chen, *ChemSusChem* **2023**, *17*, 202301228.
[165] Y. Li, T. Gao, D. Ni, Y. Zhou, M. Yousaf, Z. Guo, J. Zhou, P. Zhou, Q. Wang, S. Guo, *Adv. Mater.* **2022**, *34*, 2107638.
[166] J. Yuan, B. Xi, P. Wang, Z. Zhang, N. Song, X. An, J. Liu, J. Feng, S. Xiong, *Small* **2022**, *18*, 2203947.
[167] R. Bai, Q. Lin, X. Li, F. Ling, H. Wang, S. Tan, L. Hu, M. Ma, X. Wu, Y. Shao, *Angew. Chem., Int. Ed.* **2023**, *135*, 202218165.
[168] X. M. Zhang, Z. W. Deng, C. H. Y. Xu, Y. Deng, Y. Jia, H. Luo, H. Wu, W. L. Cai, Y. Zhang, *Adv. Energy Mater.* **2023**, *13*, 2302749.
[169] Y. Tao, S. W. Zuo, S. H. Xiao, P. X. Sun, N. W. Li, J. S. Chen, H. B. Zhang, L. Yu, *Small* **2022**, *18*, 2203231.
[170] Z. Q. Yan, Z. H. Sun, Z. H. Guo, H. S. Liu, Y. Qiu, L. Qian, *ACS Appl. Energy Mater.* **2022**, *5*, 8563.
[171] L. P. Si, J. Y. Wang, Z. C. Lu, Z. D. Chen, L. J. Zhang, H. Y. Liu, *ACS Appl. Energy Mater.* **2022**, *5*, 8554.
[172] H. C. Lin, J. L. Hong, *ACS Appl. Energy Mater.* **2022**, *5*, 11304.
[173] Z. D. Guo, Y. F. Zhao, Y. Q. Miao, D. S. Wang, D. Zhang, *ACS Appl. Energy Mater.* **2022**, *5*, 11844.
[174] W. Zhang, H. Pan, N. Han, S. H. Feng, X. Zhang, W. Guo, P. P. Tan, S. J. Xie, Z. Y. Zhou, Q. R. Ma, X. L. Guo, A. Vlad, M. Wubbenhorst, J. S. Luo, J. Fransaer, *Adv. Energy Mater.* **2023**, *13*, 2301551.
[175] Z. Xu, X. Z. Guo, W. J. Song, J. Z. Wang, T. T. Qin, Y. F. Yuan, J. Lu, *Adv. Mater.* **2023**, *36*, 2303612.
[176] T. Wang, J. R. He, Z. Zhu, X. B. Cheng, J. Zhu, B. A. Lu, Y. P. Wu, *Adv. Mater.* **2023**, *35*, 2303520.
[177] C. X. Dong, C. Zhou, M. W. Wu, Y. K. Yu, K. S. Yu, K. J. Yan, C. L. Shen, J. P. Gu, M. Y. Yan, C. L. Sun, L. Q. Mai, X. Xu, *Adv. Energy Mater.* **2023**, *13*, 2301505.
[178] T. Huang, Y. Sun, J. Wu, J. Jin, C. Wei, Z. Shi, M. Wang, J. Cai, X.-T. An, P. Wang, *ACS Nano* **2021**, *15*, 14105.
[179] Y. Li, J. Wu, B. Zhang, W. Wang, G. Zhang, Z. W. Seh, N. Zhang, J. Sun, L. Huang, J. Jiang, *Energy Storage Mater.* **2020**, *30*, 250.
[180] Y. Feng, L. Zu, S. Yang, L. Chen, K. Liao, S. Meng, C. Zhang, J. Yang, *Adv. Funct. Mater.* **2022**, *32*, 2207579.
[181] H. Shi, X. Ren, J. Lu, C. Dong, J. Liu, Q. Yang, J. Chen, Z. S. Wu, *Adv. Energy Mater.* **2020**, *10*, 2002271.
[182] R. Wang, R. Wu, X. Yan, D. Liu, P. Guo, W. Li, H. Pan, *Adv. Funct. Mater.* **2022**, *32*, 2200424.
[183] Y. Zhang, J. Liu, J. Wang, Y. Zhao, D. Luo, A. Yu, X. Wang, Z. Chen, *Angew. Chem., Int. Ed.* **2021**, *133*, 26826.
[184] D. Guo, X. Zhang, M. Liu, Z. Yu, X. a. Chen, B. Yang, Z. Zhou, S. Wang, *Adv. Funct. Mater.* **2022**, *32*, 2204458.
[185] Z. Han, S. Zhao, J. Xiao, X. Zhong, J. Sheng, W. Lv, Q. Zhang, G. Zhou, H. M. Cheng, *Adv. Mater.* **2021**, *33*, 2105947.
[186] D. Zhang, S. Wang, R. Hu, J. Gu, Y. Cui, B. Li, W. Chen, C. Liu, J. Shang, S. Yang, *Adv. Funct. Mater.* **2020**, *30*, 2002471.
[187] C. Zhou, M. Li, N. Hu, J. Yang, H. Li, J. Yan, P. Lei, Y. Zhuang, S. Guo, *Adv. Funct. Mater.* **2022**, *32*, 2204635.
[188] S. Qiao, D. Lei, Q. Wang, X. Shi, Q. Zhang, C. Huang, A. Liu, G. He, F. Zhang, *Chem. Eng. J.* **2022**, *442*, 136258.
[189] Y. Ma, T. Wu, Y. Jiao, F. Wang, B. Chen, Y. Yan, A. Hu, Y. Li, Y. Fan, M. He, *Small* **2022**, *18*, 2205470.
[190] D. Wang, K. Ma, J. Hao, W. Zhang, H. Shi, C. Wang, Z. Xiong, Z. Bai, F.-R. Chen, J. Guo, *Chem. Eng. J.* **2023**, *466*, 143182.
[191] Z. Wang, Y. Cheng, S. Wang, J. Xu, B. Peng, D. Luo, L. Ma, *Nano Res.* **2023**, *16*, 9335.
[192] G. Zhao, Q. Chen, L. Wang, T. Yan, H. Li, C. Yuan, J. Mao, X. Feng, D. Sun, L. Zhang, *J. Mater. Chem. A* **2022**, *10*, 19893.
[193] L. Ma, J. Qian, Y. Li, Y. Cheng, S. Wang, Z. Wang, C. Peng, K. Wu, J. Xu, I. Manke, *Adv. Funct. Mater.* **2022**, *32*, 2208666.
[194] P. Song, S. Zheng, Z. Ullah, Z. Yang, P. Zhu, A. He, C. Wang, Q. Li, *ACS Appl. Energy Mater.* **2023**, *6*, 4671.
[195] C. Xiao, W. Song, J. Liang, J. Zhang, Z. Huang, J. Zhang, H. Wang, C. Zhong, J. Ding, W. Hu, *J. Mater. Chem. A* **2022**, *10*, 3667.
[196] W.-H. Lai, H. Wang, L. Zheng, Q. Jiang, Z.-C. Yan, L. Wang, H. Yoshikawa, D. Matsumura, Q. Sun, Y.-X. Wang, Q. Gu, J.-Z. Wang, H.-K. Liu, S.-L. Chou, S.-X. Dou, *Angew. Chem., Int. Ed.* **2020**, *59*, 22171.
[197] H. Liu, W.-H. Lai, Y. Liang, X. Liang, Z.-C. Yan, H.-L. Yang, Y.-J. Lei, P. Wei, S. Zhou, Q.-F. Gu, S.-L. Chou, H. K. Liu, S. X. Dou, Y.-X. Wang, *J. Mater. Chem. A* **2021**, *9*, 566.
[198] F. Xiao, H. Wang, J. Xu, W. Yang, X. Yang, D. Y. W. Yu, A. L. Rogach, *Adv. Energy Mater.* **2021**, *11*, 2100989.
[199] M. S. Nahian, R. Jayan, M. M. Islam, *ACS Catal.* **2022**, *12*, 7664.
[200] E. Zhang, X. Hu, L. Meng, M. Qiu, J. Chen, Y. Liu, G. Liu, Z. Zhuang, X. Zheng, L. Zheng, Y. Wang, W. Tang, Z. Lu, J. Zhang, Z. Wen, D. Wang, Y. Li, *J. Am. Chem. Soc.* **2022**, *144*, 18995.
[201] R. Bai, Q. Lin, X. Li, F. Ling, H. Wang, S. Tan, L. Hu, M. Ma, X. Wu, Y. Shao, X. Rui, E. Hu, Y. Yao, Y. Yu, *Angew. Chem., Int. Ed.* **2023**, *62*, 202218165.
[202] D. Fang, S. Huang, T. Xu, P. Sun, X. L. Li, Y. V. Lim, D. Yan, Y. Shang, B.-J. Su, J.-Y. Juang, Q. Ge, H. Y. Yang, *ACS Appl. Mater. Interfaces* **2023**, *15*, 26650.
[203] Y. Jiang, Z. Yu, X. Zhou, X. Cheng, H. Huang, F. Liu, Y. Yang, S. He, H. Pan, H. Yang, Y. Yao, X. Rui, Y. Yu, *Adv. Mater.* **2023**, *35*, 2208873.
[204] N. Li, Y. Zhan, H. Wu, J. Fan, J. Jia, *Nanoscale* **2023**, *15*, 2747.
[205] B.-W. Zhang, L. Cao, C. Tang, C. Tan, N. Cheng, W.-H. Lai, Y.-X. Wang, Z.-X. Cheng, J. Dong, Y. Kong, S.-X. Dou, S. Zhao, *Adv. Mater.* **2023**, *35*, 2206828.
[206] M. Jakhar, V. Barone, Y. Ding, *Nanoscale* **2024**, *16*, 12982.
[207] Y.-J. Lei, X. Lu, H. Yoshikawa, D. Matsumura, Y. Fan, L. Zhao, J. Li, S. Wang, Q. Gu, H.-K. Liu, S.-X. Dou, S. Devaraj, T. Rojo, W.-H. Lai, M. Armand, Y.-X. Wang, G. Wang, *Nat. Commun.* **2024**, *15*, 3325.
[208] Z. Li, X. Chen, G. Yao, L. Wei, Q. Chen, Q. Luo, F. Zheng, H. Wang, *Adv. Funct. Mater.* **2024**, *34*, 2400859.
[209] J. Ruan, Y.-J. Lei, Y. Fan, M. C. Borras, Z. Luo, Z. Yan, B. Johannessen, Q. Gu, K. Konstantinov, W. K. Pang, W. Sun, J.-Z. Wang, H.-K. Liu, W.-H. Lai, Y.-X. Wang, S.-X. Dou, *Adv. Mater.* **2024**, *36*, 2312207.
[210] C. Wang, Q. Xiao, X. Yang, H. Yan, J. Qi, S. Liu, J. Wang, *Ceram. Int.* **2024**, *50*, 6898.
[211] S. Wu, C. Wang, H. Liang, W. Nong, Z. Zeng, Y. Li, C. Wang, *Small* **2024**, *20*, 2305161.
[212] G. Yao, Z. Li, Y. Zhang, Y. Xiao, L. Wei, H. Niu, Q. Chen, Y. Yang, F. Zheng, *Adv. Funct. Mater.* **2024**, *34*, 2214353.
[213] X. Zhong, Y. Huang, J. Cai, Y. Li, Z. He, D. Cai, Z. Geng, W. Deng, G. Zou, H. Hou, X. Ji, *J. Am. Chem. Soc.* **2024**, *146*, 32124.

[214] G. Wu, T. Liu, Z. Lao, Y. Cheng, T. Wang, J. Mao, H. Zhang, E. Liu, C. Shi, G. Zhou, C. He, W. Hu, N. Zhao, N. Wu, B. Chen, *Angew. Chem., Int. Ed.* **2025**, *64*, 202422208.
[215] F. Zheng, Y. Zhang, Z. Li, G. Yao, L. Wei, C. Wang, Q. Chen, H. Wang, *Nat. Commun.* **2025**, *16*, 4372.
[216] X. R. Dong, W. Y. Shi, G. Wang, J. W. Chen, R. L. Wang, J. Zhang, *Small* **2023**, *30*, 2307407.
[217] X. R. Cheng, Y. Jiang, J. H. Qu, C. F. Li, K. Zhang, Y. A. Zhang, B. J. Wang, H. S. Peng, *Sci. China Mater.* **2023**, *66*, 4615.
[218] W. Zhao, J. Wang, R. Yin, B. Li, X. Huang, L. Zhao, L. Qian, *J. Colloid Interface Sci.* **2020**, *564*, 28.
[219] J. Zheng, W. Zhang, R. Wang, J. Wang, Y. Zhai, X. Liu, *Small* **2023**, *19*, 2204559.
[220] Z. Lian, Y. Lu, S. Ma, Z. Li, Q. Liu, *Chem. Eng. J.* **2022**, *445*, 136852.
[221] W. Y. Noh, E. M. Kim, K. Y. Kim, J. H. Kim, H. Y. Jeong, P. Sharma, G. Lee, J.-W. Jang, S. H. Joo, J. S. Lee, *J. Mater. Chem. A* **2020**, *8*, 18891.
[222] H. Sun, Q. Liu, Z. Gao, L. Geng, Y. Li, F. Zhang, J. Yan, Y. Gao, K. Suenaga, L. Zhang, *J. Mater. Chem. A* **2022**, *10*, 6096.
[223] M. Wang, H. Ji, S. Liu, H. Sun, J. Liu, C. Yan, T. Qian, *Chem. Eng. J.* **2020**, *393*, 124702.
[224] S. Liu, H. Ji, M. Wang, H. Sun, J. Liu, C. Yan, T. Qian, *ACS Appl. Mater. Interfaces* **2020**, *12*, 15298.
[225] Q. Wang, Q. Feng, Y. Lei, S. Tang, L. Xu, Y. Xiong, G. Fang, Y. Wang, P. Yang, J. Liu, *Nat. Commun.* **2022**, *13*, 3689.
[226] R. Xu, X. Wang, C. Zhang, Y. Zhang, H. Jiang, H. Wang, G. Su, M. Huang, A. Toghan, *Chem. Eng. J.* **2022**, *433*, 133685.
[227] M. Arif Khan, C. Sun, J. Cai, D. Ye, K. Zhao, G. Zhang, S. Shi, L. Ali Shah, J. Fang, C. Yang, *ChemElectroChem* **2021**, *8*, 1298.
[228] J. Sheng, S. Zhu, G. Jia, X. Liu, Y. Li, *Nano Res.* **2021**, *14*, 4541.
[229] H. Li, K. Du, C. Xiang, P. An, X. Shu, Y. Dang, C. Wu, J. Wang, W. Du, J. Zhang, *J. Mater. Chem. A* **2020**, *8*, 17136.
[230] H. S. Kim, J. Lee, J.-H. Jang, H. Jin, V. K. Paidi, S.-H. Lee, K.-S. Lee, P. Kim, S. J. Yoo, *Appl. Surf. Sci.* **2021**, *563*, 150208.
[231] Y. Ma, H. Fan, C. Wu, M. Zhang, J. Yu, L. Song, K. Li, J. He, *Carbon* **2021**, *185*, 526.
[232] Y. B. Zhu, P. Z. Li, X. J. Yang, M. Q. Wang, Y. L. Zhang, P. K. Gao, Q. K. Huang, Y. Wei, X. Yang, D. Y. Wang, Y. Shen, M. K. Wang, *Adv. Energy Mater.* **2023**, *13*, 2204143.
[233] C. F. Xu, Y. L. Dong, H. P. Zhao, Y. Lei, *Adv. Funct. Mater.* **2023**, *33*, 2300926.
[234] Z. Wang, B. Liu, X. Yang, C. T. Zhao, P. Dong, X. Li, Y. N. Zhang, K. Doyle-Davis, X. Y. Zeng, Y. J. Zhang, X. L. Sun, *Adv. Funct. Mater.* **2023**, *33*, 2213931.
[235] C. Guo, F. L. Zhang, X. Han, L. P. Zhang, Q. Hou, L. L. Gong, J. C. Wang, Z. H. Xia, J. H. Hao, K. Y. Xie, *Adv. Mater.* **2023**, *35*, 2302325.
[236] Y.-J. Rho, B. Kim, K. Shin, G. Henkelman, W.-H. Ryu, *J. Mater. Chem. A* **2022**, *10*, 19710.
[237] J. Lin, J. Ding, H. Wang, X. Yang, X. Zheng, Z. Huang, W. Song, J. Ding, X. Han, W. Hu, *Adv. Mater.* **2022**, *34*, 2200559.
[238] L. Zhou, H. Wang, K. Zhang, Y. Qi, C. Shen, T. Jin, K. Xie, *Sci. China Mater.* **2021**, *64*, 2139.
[239] L. Liu, Z. Du, J. Sun, S. He, K. Wang, M. Li, L. Xie, W. Ai, *Small* **2023**, *19*, 2300556.
[240] M. Liang, H. Xie, E. Liu, C. Shi, C. He, N. Zhao, *Carbon* **2022**, *196*, 795.
[241] J. Wang, J. Zhang, S. Cheng, J. Yang, Y. Xi, X. Hou, Q. Xiao, H. Lin, *Nano Lett.* **2021**, *21*, 3245.
[242] Y. Li, P. Zhou, H. Li, T. Gao, L. Zhou, Y. Zhang, N. Xiao, Z. Xia, L. Wang, Q. Zhang, *Small Methods* **2020**, *4*, 1900701.

**Jianan Gu** received his Ph.D. in Materials Science from Beihang University in 2020. He is currently an associate professor at North China Electric Power University. During the period from 2024.7 to 2025.5, he was a research consultant in Huabin Zhang's group in KAUST. His research interests focus on the synthesis of 2D materials and their applications in energy storage and catalysis, including MXenes, Li/Na metal anodes, and Zn-ion batteries.

**Yuanfu Ren** received his B.Eng. and M.Sc. degrees from Central South University in 2018 and 2021. He is currently a Ph.D. student in chemistry at the King Abdullah University of Science and Technology (KAUST). His research is centered on fundamental electrochemistry and the development of advanced electrochemical techniques for key catalytic reactions in energy conversion processes.

**Meicheng Li** received his Ph.D. from Harbin Institute of Technology in 2001. During the period from 2004 to 2006, he was a visiting scholar in the University of Cambridge. He currently is dean, professor, and Ph.D. supervisor of the School of New Energy at North China Electric Power University. His research interests focus on solar cells and solar energy utilization technology, lithium/sodium ion batteries and energy storage technology, and micro energy and smart energy systems.

**Huabin Zhang** received his Ph.D. degree in chemistry from the Fujian Institute of Research on the Structure of Matter, Chinese Academy of Sciences (FJIRSM-CAS). After finishing his postdoc research in Japan (Supervisor: Jinhua Ye) at the National Institute of Materials Science (NIMS) and Singapore (Supervisor: Xiong Wen Lou) at Nanyang Technological University, Singapore, he joined KAUST serving as an assistant professor in January 2021. His research interests focus on advanced catalysis for sustainable energy.